From EMC- and Cronin-effects to signals of quark-gluon plasma

Wei Zhu[1,2], **Jianhong Ruan**[1] and **Fengyao Hou**[2]

[1]Department of Physics, East China Normal University, Shanghai 200062, P.R. China

[2]Kavli Institute for Theoretical Physics China, CAS, Beijing 100190, P.R. China

Abstract

The EMC- and Cronin-effects are explained by a unitarized evolution equation, where the shadowing and antishadowing corrections are dynamically produced by gluon fusions. For this sake, an alternative form of the GLR-MQ-ZRS equation is derived. The resulting integrated and unintegrated gluon distributions in proton and nuclei are used to analyze the contributions of the initial parton distributions to the nuclear suppression factor in heavy ion collisions. A simulation of the fractional energy loss is extracted from the RHIC and LHC data, where the contributions of the nuclear shadowing and antishadowing effects are considered. We find a rapid crossover from week energy loss to strong energy loss at a universal critical energy of gluon jet $E_c \sim 10GeV$.

PACS number(s): 24.85.+p; 12.38.-t; 13.60.Hb

keywords: Quark gluon plasma; Nuclear gluon distribution; Energy loss

1 Introduction

One of the important findings at RHIC and LHC is that high transverse momentum k_t hadron production in central heavy ion collisions is suppressed compared to p+p collisions [1, 2]. This suppression can be attributed to energy loss of high-k_t partons that traverse the hot and dense medium (i.e., quark-gluon plasma QGP) formed in these collisions. An important goal of the study of heavy ion collisions is therefore to determine the properties QGP from the measured fractional energy loss after deducting nuclear effects on the initial parton distributions.

The parton densities in a bound nucleon differ from that in a free nucleon. One of such examples is that the ratio of nuclear and deuterium's structure functions is smaller or larger than unity at Bjorken variable $x < 0.1$ or $0.1 < x < 0.3$. These two facts are called as the nuclear shadowing and antishadowing in the EMC effect [3]. The nuclear shadowing and antishadowing effects origin from the gluon fusion (recombination) between two different nucleons in a nucleus, which changes the distributions of gluon and quarks, but does not change their total momentum [4]. In consequence, the lost gluon momentum in the shadowing range should be compensated in terms of new gluons with larger x, which forms the antishadowing effect.

An other example is the Cronin effect: the ratio of particle yields in $d + A$ (scaled by the number of collisions)$/p + p$, exceeds unity in an intermediate transverse momentum range (Cronin enhancement) and is bellow unity at smaller transverse momentum (anti-Cronin suppression). This effect was first seen at lower fixed target energies [5] and has been confirmed in $\sqrt{s} = 200GeV$ $d + Au$ collisions at the BNL Relativistic Heavy Ion Collider (RHIC) [6].

The Cronin effect is more complicated than the EMC effect, the former mixes the shadowing-antishadowing corrections at initial state and the medium modifications at

final state. The later is an important information for understanding the properties of dense and hot matter formed in high-energy heavy-ion collisions. Therefore, the nuclear shadowing and antishadowing effects, which have appeared in the EMC effect, should be extracted from the Cronin effect, then the remaining result exposes the medium properties.

The saturation models are broadly used to study the Cronin effect. The saturation is a limiting behavior of the shadowed gluon distribution in the Jalilian-Marian-Iancu-McLerran-Weigert-Leonidov-Kovner (JIMWLK) equation [7], where the unintegrated gluon distribution is absolutely flat in k_t-space at $k_t < Q_s$, Q_s is the saturation scale. An elemental QCD process, which arises nonlinear corrections in the JIMWLK equation is also the gluon fusion $gg \to g$. As we have pointed out that the antishadowing effect always coexists with the shadowing effect in *any gluon fusion processes* due to a general restriction of momentum conservation [8]. However, such antishadowing effect is completely neglected in the original saturation models. The Cronin enhancement in these models, (i) is additionally explained as multiple scattering [9] using the Glauber-Mueller model [10], or the McLerran-Venugopalan model [11]; (ii) is produced by special initial gluon distributions of proton and nucleus [12]. A following question is: what are the nuclear antishadowing contributions to the Cronin effect?

A global Dokshitzer-Gribov-Lipatov-Altarelli-Parisi (DGLAP) analysis of nuclear parton distribution functions (for example, the ESP09-set [13]) was proposed, where the data from deep inelastic scattering (DIS), Drell-Yan dilepton production, and inclusive high-k_t hadron production data measured at RHIC are used. They found that a strong gluon antishadowing effect is necessary to support the RHIC data. However, the shadowing and antishadowing effects in the DGLAP analysis are phenomenologically assumed in the initial conditions, since the DGLAP equation [14] does not contain the nonlinear corrections of gluon fusion. Due to the lack of the experimental data about nuclear gluon

distribution, the above mentioned status are undetermined. For example, a similar global DGLAP analysis shows that the available data are not enough to fix these complicated input distributions and even appearing or not the antishadowing effect are uncertain [15]. Besides, the DGLAP equation in the collinear factorization scheme evolves the integrated parton distributions, the behavior of the unintegrated gluon distributions, which contain information of the transverse momentum distribution is completely undefined in this method. Therefore, the ESP09-set of nuclear parton distributions can not predict the RHIC data at lower k_t, where the contributions from intrinsic transverse momentum become important [13].

The modification of the gluon recombination to the standard DGLAP evolution equation was first proposed by Gribov-Levin-Ryskin and Mueller-Qiu (the GLR-MQ equation) in [16,17], and it is naturally regarded as the QCD dynamics of the nuclear shadowing since the same gluon fusion exists both in proton and in nucleus, and they differ only by the strength of the nonlinear terms [18]. However, the GLR-MQ equation does not predict the nuclear antishadowing effect since the momentum conservation is violated in this equation. This defect of the GLR-MQ equation is corrected by a modified equation (the GLR-MQ-ZRS equation) by Zhu, Ruan and Shen in [19,20], where the corrections of the gluon fusion to the DGLAP equation lead to the shadowing and antishadowing effects. Unfortunately, the integral solutions in the present GLR-like equations need the initial distributions on a boundary line (x, Q_0^2) at a fixed Q_0^2, and they still contain the unknown input with nuclear shadowing and antishadowing effects at small x.

Motivation of this work is trying to improve the above questionable methods. We shall study the nuclear shadowing and antishadowing effects in the EMC- and Cronin-effects, which are dynamically arisen from the gluon recombination. Then we use the resulting nuclear gluon distributions to predict the contributions of the initial parton distributions

to the nuclear suppression factor in heavy ion collisions and to extract fractional energy loss from the RHIC and LHC data. For this sake, an alternative form of the GLR-MQ-ZRS equation at the double-leading-logarithmic-approximation (DLLA) is derived in Sec. 2. The evolution of this equation is along small x-direction. The nonlinear corrections to the input distributions may neglected if the value of the starting point x_0 is large enough. The shadowing and antishadowing effects are naturally grown up in the evolution at $x < x_0$. Thus, we avoid the unperturbative nuclear modifications in the input distributions and simplify the initial conditions. We use the existing data about the EMC- and Cronin-effects to fix a few of free parameters in the solutions. Then the resulting integrated and unintegrated gluon distributions in proton and nuclei are used to analyze the nuclear suppression factor in heavy ion collisions.

Our main conclusions are: (i) we support the stronger shadowing-antishadowing effects in the heavy nucleus both in the unintegrated and integrated gluon distributions due to a strong A-dependence of the nonlinear corrections; (ii) the anti-Cronin suppression and Cronin enhancement mainly origin from the same gluon recombination mechanism as in the nuclear shadowing and antishadowing effects of the EMC effect; (iii) fractional energy loss is rapid crossover from week energy loss to strong energy loss at a universal critical energy of gluon jet $E_c \sim 10GeV$.

The organizations of this work are as follows. We shall derive the GLR-MQ-ZRS equation in a new form in Sec.2. Using this equation we study the shadowing and antishadowing effects in the EMC effect in Sec.3. These resulting unintegrated gluon distributions in proton and nuclei are used to expose the nuclear shadowing and antishadowing contributions to the Cronin effect in Sec.4. The nuclear shadowing and antishadowing effects to the nuclear suppression factor are predicted and a simulations of fractional energy loss is extracted from the RHIC and LHC data in Sec. 5.

2 A new form of the GLR-MQ-ZRS equation

In history, the DGLAP evolution is derived by using the renormalization group method for the integrated distributions. The resulting equation evolves with factorization scale μ. In this section, we try to write the DGLAP equation with the nonlinear modifications beginning from the unintegrated distributions. Then, we get an alternative form of these equations, which evolves with the Bjorken variable x.

We begin from a deeply inelastic scattering process, where the unintegrated gluon distribution is measured. In the k_t-factorization scheme, the cross section is decomposed into

$$\begin{aligned} & d\sigma(probe^* P \to kX) \\ &= f(x_1, k_{1t}^2) \otimes \mathcal{K}\left(\frac{k_t^2}{k_{1t}^2}, \frac{x}{x_1}, \alpha_s\right) \otimes d\sigma(probe^* k_1 \to k) \\ &\equiv \Delta f(x, k_t^2) \otimes d\sigma(probe^* k_1 \to k), \end{aligned} \tag{1}$$

which contains the evolution kernel $\mathcal{K}$, the unintegrated gluon distribution function f and the $probe^*$-parton cross section $d\sigma(probe^* k_1 \to k)$. For simplicity, we take the fixed QCD coupling at the leading order (LO) approximation in this work. According to the scale-invariant parton picture of the renormalization group [21], we regard $\Delta f(x, k_t^2)$ as the increment of the distribution $f(x_1, k_{1t}^2)$ when it evolves from (x_1, k_{1t}^2) to (x, k_t^2). Thus, the connection between two functions $f(x_1, k_{1t}^2)$ and $f(x, k_t^2)$ via Eq. (1) is

$$\begin{aligned} f(x, k_t^2) &= f(x_1, k_{1t}^2) + \Delta f(x, k_t^2) \\ &= f(x_1, k_{1t}^2) + \int_{k_{1t,min}^2}^{k_t^2} \frac{dk_{1t}^2}{k_{1t}^2} \int_x^1 \frac{dx_1}{x_1} \mathcal{K}\left(\frac{k_t^2}{k_{1t}^2}, \frac{x}{x_1}, \alpha_s\right) f(x_1, k_{1t}^2). \end{aligned} \tag{2}$$

In the case of the LO DGLAP evolution, we adopt a physical (axial) gauge, which sums over only the transverse gluon polarizations, so that the ladder-type diagrams dominate

the evolution, the unintegrated distributions satisfy the normalization relation

$$G(x,\mu^2) \equiv xg(x,\mu^2) = \int_{k_{t,min}^2}^{\mu^2} \frac{dk_t^2}{k_t^2} xf(x,k_t^2) \equiv \int_{k_{t,min}^2}^{\mu^2} \frac{dk_t^2}{k_t^2} F(x,k_t^2), \tag{3}$$

where the possible non-logarithmic tail for $k_t > \mu$ are beyond NLO accuracy. These distributions correspond to the density of partons in the proton with longitudinal momentum fraction x, integrated over the parton transverse momentum up to $k_t = \mu$.

From Eqs. (2) and (3), we have

$$\Delta g(x,\mu^2) = \int_{k_{t,min}^2}^{\mu^2} \frac{dk_t^2}{k_t^2} \int_{k_{1t,min}^2}^{k_t^2} \frac{dk_{1t}^2}{k_{1t}^2} \int_x^1 \frac{dx_1}{x_1} \frac{1}{x_1} \mathcal{K}\left(\frac{k_t^2}{k_{1t}^2}, \frac{x}{x_1}, \alpha_s\right) F(x_1, k_{1t}^2), \tag{4}$$

or

$$\begin{aligned}\Delta G(x,\mu^2) = \Delta xg(x,\mu^2) &= \int_{k_{T,min}^2}^{\mu^2} \frac{dk_t^2}{k_t^2} \int_{k_{1t,min}^2}^{k_t^2} \frac{dk_{1t}^2}{k_{1t}^2} \int_x^1 \frac{dx_1}{x_1} \frac{x}{x_1} \mathcal{K}\left(\frac{k_t^2}{k_{1t}^2}, \frac{x}{x_1}, \alpha_s\right) F(x_1, k_{1t}^2) \\ &= \int_{k_{t,min}^2}^{\mu^2} \frac{dk_t^2}{k_t^2} \int_x^1 \frac{dx_1}{x_1} \frac{x}{x_1} \mathcal{K}\left(\frac{x}{x_1}, \alpha_s\right) G(x_1, k_t^2),\end{aligned} \tag{5}$$

where the last step is held when the k_t-strong ordered. Usually DGLAP evolution is written in terms of the virtuality k^2 rather than k_t^2 , but at LO level this is the same since the difference is a NLO effect. Therefore, we take

$$G(x,k_t^2) \to G(x,\mu^2). \tag{6}$$

Thus, in

$$G(x,\mu^2) = G(x_1,\mu_1^2) + \Delta G(x,\mu^2), \tag{7}$$

we write

$$\Delta G(x,\mu^2)$$

$$= \int_{\mu^2_{1,min}}^{\mu^2} \frac{d\mu_1^2}{\mu_1^2} \int_x^1 \frac{dx_1}{x_1} \frac{x}{x_1} \mathcal{K}^{LL(\mu^2)}_{DGLAP}(\frac{x}{x_1}, \alpha_s) G(x_1, \mu_1^2), \tag{8}$$

at the leading logarithmic μ^2 approximation, in which the unregularized splitting kernels

$$\begin{aligned} \frac{dx_1}{x_1}\mathcal{K}^{LL(\mu^2)}_{DGLAP} &= \frac{\alpha_s N_c}{\pi}\frac{dx_1}{x_1}[z(1-z) + \frac{1-z}{z} + \frac{z}{1-z}] \\ &= \frac{\alpha_s N_c}{\pi}\frac{dx_1}{x_1}\left[\frac{x(x_1-x)}{x_1^2} + \frac{x_1-x}{x} + \frac{x}{x_1-x}\right] \qquad (9a) \\ &\overset{x\ll x_1}{\longrightarrow} \frac{dx_1}{x_1}\mathcal{K}^{DLL}_{DGLAP} = \frac{\alpha_s N_c}{\pi}\frac{dx_1}{x}. \qquad (9b) \end{aligned}$$

We add the contributions of the nonlinear recombination terms in Eq. (8) according to Refs. [19, 20] (See appendix A),

$$\begin{aligned} &\Delta G(x,\mu^2) \\ &= \int_{\mu^2_{1,min}}^{\mu^2} \frac{d\mu_1^2}{\mu_1^2} \int_x^1 \frac{dx_1}{x_1} \frac{x}{x_1} \mathcal{K}^{LL(\mu^2)}_{DGLAP}(\frac{x}{x_1}, \alpha_s) G(x_1, \mu_1^2) \\ &-2\int_{\mu^2_{1min}}^{Q^2} \frac{d\mu_1^2}{\mu_1^4} \int_x^{1/2} \frac{dx_1}{x_1} \frac{x}{x_1} \mathcal{K}^{GG\to GG,\ LL(\mu^2)}_{GLR-MQ-ZRS}\left(\frac{x}{x_1}, \alpha_s\right) G^{(2)}(x_1, \mu_1^2) \\ &+\int_{\mu^2_{1min}}^{\mu^2} \frac{d\mu_1^2}{\mu_1^4} \int_{x/2}^{1/2} \frac{dx_1}{x_1} \frac{x}{x_1} \mathcal{K}^{GG\to GG,\ LL(\mu^2)}_{GLR-MQ-ZRS}\left(\frac{x}{x_1}, \alpha_s\right) G^{(2)}(x_1, \mu_1^2), \end{aligned} \tag{10}$$

where

$$\begin{aligned} &\frac{dx_1}{x_1}\mathcal{K}^{GG\to GG,\ LL(\mu^2)}_{GLR-MQ-ZRS} \\ &= \frac{\alpha_s^2}{8}\frac{N_c^2}{N_c^2-1}\frac{(2x_1-x)(72x_1^4 - 48x_1^3 x + 140x_1^2x^2 - 116x_1x^3 + 29x^4)}{x_1^5 x}dx_1 \qquad (11a) \\ &\overset{x\ll x_1}{\longrightarrow} \frac{dx_1}{x_1}\mathcal{K}^{GG\to GG,\ DLL}_{GLR-MQ-ZRS} = 18\alpha_s^2\frac{N_c^2}{N_c^2-1}\frac{dx_1}{x}. \qquad (11b) \end{aligned}$$

$$G^{(2)}(x,\mu^2) = R_G G^2(x,\mu^2), \tag{12}$$

where $R_G = 1/(\pi R^2)$ is a correlation coefficient with the dimension $[L^{-2}]$, R is the effective correlation length of two recombination gluons. One can easily get the GLR-MQ-ZRS equation at DLL approximation

$$\frac{\partial G(x,\mu^2)}{\partial \ln \mu^2}$$
$$= \frac{\alpha_s N_c}{\pi}\int_x^1 \frac{dx_1}{x_1} G(x_1,\mu^2) - \frac{36\alpha_s^2}{\pi\mu^2 R^2}\frac{N_c^2}{N_c^2-1}\int_x^{1/2}\frac{dx_1}{x_1}G^2(x_1,\mu^2)$$
$$+\frac{18\alpha_s^2}{\pi\mu^2 R^2}\frac{N_c^2}{N_c^2-1}\int_{x/2}^{1/2}\frac{dx_1}{x_1}G^2(x_1,\mu^2). \quad (13)$$

It is interesting to compare this small-x version of the GLR-MQ-ZRS equation with the GLR-MQ equation, which is [17]

$$\frac{\partial G(x,\mu^2)}{\partial \ln \mu^2}$$
$$= \frac{\alpha_s N_c}{\pi}\int_x^1 \frac{dx_1}{x_1} G(x_1,\mu^2) - \frac{36\alpha_s^2}{8\mu^2 R^2}\frac{N_c^2}{N_c^2-1}\int_x^{1/2}\frac{dx_1}{x_1}G^2(x_1,\mu^2), \quad (14)$$

where

$$G^{(2)}(x,\mu^2) = \frac{9}{8\pi R^2}G^2(x,\mu^2), \quad (15)$$

is assumed.

Comparing with the GLR-MQ equation (14), there are several features in the GLR-MQ-ZRS equation (13): (i) the momentum conservation of partons is restored in Eq. (13); (ii) because of the shadowing and antishadowing effects in Eq. (13) have different kinematic regions, the net effect depends not only on the local value of the gluon distribution at the observed point, but also on the shape of the gluon distribution when the Bjorken variable goes from x to $x/2$. In consequence, the shadowing effect in the evolution process will be obviously weakened by the antishadowing effect if the distribution is steeper. Therefore, the antishadowing effect can not be neglected in the pre-saturation range.

According to the definition Eq. (3), one can roughly estimate the unintegrated gluon distribution using

$$F(x,k_t^2) \simeq \mu^2 \frac{\partial G(x,\mu^2)}{\partial \mu^2}\bigg|_{\mu^2=k_t^2}. \tag{16}$$

However, Eq. (16) cannot remain true as x increases, since the negative virtual DGLAP term may exceed the real emission DGLAP contribution and it would give negative values of F. In fact, due to strong k_t ordering in DGLAP evolution, the transverse momentum of the final parton is obtained, to leading-order accuracy, just at the final step of the evolution. Thus, the k_t-dependent distribution can be calculated directly from the DGLAP equation keeping only the contribution which corresponds to a single real emission, while all the virtual contributions from a scale equal to k_t up to the final scale μ of the hard subprocess are resummed into a Sudakov factor T. The factor T describes the probability that during the evolution there are no parton emissions. However, at the small x range, the virtual contributions to the gluon distribution in the DGLAP kernel can be neglected. Besides, we have indicated that the contributions of the virtual processes in the nonlinear kernels of the GLR-MQ-ZRS equation are canceled [19], therefore, the Sudakov form factors are same in nucleon and nucleus [22] and they are really canceled in the following ratio form. Thus, we use

$$\begin{aligned}
&\Delta G(x,\mu^2) \\
&= \int_{k_{min}^2}^{\mu^2} \frac{dk_t^2}{k_t^2} \int_{k_{1t,min}^2}^{k_t^2} \frac{dk_{1t}^2}{k_{1t}^2} \int_x^1 \frac{dx_1}{x_1} \frac{x}{x_1} \mathcal{K}_{DGLAP}^{DLL}(\frac{x}{x_1},\alpha_s) F(x_1,k_{1t}^2) \\
&-2\int_{\mu_{1min}^2}^{\mu^2} \frac{dk_t^2}{k_t^4} \int_x^{1/2} \frac{dx_1}{x_1} \frac{x}{x_1} \mathcal{K}_{MD-DGLAP}^{DLL}\left(\frac{x}{x_1},\alpha_s\right) G^{(2)}(x_1,k_t^2) \\
&+\int_{\mu_{1min}^2}^{\mu^2} \frac{dk_t^2}{k_t^4} \int_{x/2}^{1/2} \frac{dx_1}{x_1} \frac{x}{x_1} \mathcal{K}_{MD-DGLAP}^{DLL}\left(\frac{x}{x_1},\alpha_s\right) G^{(2)}(x_1,k_t^2),
\end{aligned} \tag{17}$$

and obtain

$$\Delta F(x,k_t^2) = \mu^2 \frac{\partial \Delta G(x,\mu^2)}{\partial \mu^2}\bigg|_{\mu^2=k_t^2}$$

$$= \frac{\alpha_s N_c}{\pi} \int_{k^2_{1t,min}}^{k^2_t} \frac{dk^2_{1t}}{k^2_{1t}} \int_x^1 \frac{dx_1}{x_1} F(x_1, k^2_{1t})$$
$$-\frac{36\alpha_s^2}{k_t^2} \frac{N_c^2}{N_c^2-1} \int_x^{1/2} \frac{dx_1}{x_1} G^{(2)}(x_1, k_t^2)$$
$$+\frac{18\alpha_s^2}{k_t^2} \frac{N_c^2}{N_c^2-1} \int_{x/2}^{1/2} \frac{dx_1}{x_1} G^{(2)}(x_1, k_t^2), \tag{18}$$

Now we re-derive the GLR-MQ-ZRS equation, but which evolves with the longitudinal momentum. We differentiate

$$F(x, k_t^2) = F(x_1, k^2_{1t}) + \Delta F(x, k_t^2), \tag{19}$$

with respect to x. Note that

$$-\frac{\partial F(x, k_t^2)}{\partial x}$$
$$= \int_{k^2_{1t,min}}^{k^2_t} \frac{dk^2_{1t}}{k^2_{1t}} \frac{1}{x_1} \mathcal{K}\left(\frac{k_t^2}{k^2_{1t}}, \frac{x}{x_1}, \alpha_s\right) F(x_1, k^2_{1t})\Big|_{x_1=x}$$
$$- \int_{k^2_{1t,mi}}^{k^2_t} \frac{dk^2_{1t}}{k^2_{1t}} \int_x^1 \frac{dx_1}{x_1^2} \frac{\partial x \mathcal{K}\left(\frac{k_t^2}{k^2_{1t}}, \frac{x}{x_1}, \alpha_s\right)}{\partial x} F(x_1, k^2_{1t}). \tag{20}$$

Generally, the resummation solution is hard to obtain from this equation. However, at the $LL(1/x)$ approximation the second term on the right-hand side of Eq. (20) vanishes. In this case, the resummation becomes simple, i.e., we have

$$-x\frac{\partial F(x, k_t^2)}{\partial x}$$
$$= \frac{\alpha_s N_c}{\pi} \int_{k_{1t,min}}^{k^2_t} \frac{dk^2_{1t}}{k^2_{1t}} F(x, k^2_{1t})$$
$$-\frac{36\alpha_s^2}{\pi R^2 k_t^2} \frac{N_c^2}{N_c^2-1} \left[\int_{k^2_{1t,min}}^{k^2_t} \frac{dk^2_{1t}}{k^2_{1t}} F(x, k^2_{1t})\right]^2 + \frac{18\alpha_s^2}{\pi R^2 k_t^2} \frac{N_c^2}{N_c^2-1} \left[\int_{k^2_{1t,min}}^{k^2_t} \frac{dk^2_{1t}}{k^2_{1t}} F\left(\frac{x}{2}, k^2_{1t}\right)\right]^2,$$
$$(x \leq 0.15);$$

$$-x\frac{\partial F(x, k_t^2)}{\partial x}$$

$$= \frac{\alpha_s N_c}{\pi}\int_{k_{1t,min}}^{k_t^2}\frac{dk_{1t}^2}{k_{1t}^2}F(x,k_{1t}^2)+\frac{18\alpha_s^2}{\pi R^2 k_t^2}\frac{N_c^2}{N_c^2-1}\left[\int_{k_{1t,min}^2}^{k_t^2}\frac{dk_{1t}^2}{k_{1t}^2}F\left(\frac{x}{2},k_{1t}^2\right)\right]^2, \quad (0.15\leq x\leq 0.3), \tag{21}$$

This is a new form of the GRL-MQ-ZRS equation. The negative and positive nonlinear terms correspond to the shadowing and antishadowing effects in the gluon recombination. Note that the shadowing and antishadowing coexist in the region $x \leq 0.15$, while there is only the antishadowing in $0.15 \leq x \leq 0.3$.

The explanation of the kinematic regions of Eq. (21) is follows. The evolution kernel of the GLR-MQ-ZRS equation (11a) is derived at LL(Q^2) approximation as same as the derivation of the DGLAP equation (9a) and they are valid in a whole x range. However the DLLA form of the GLR-MQ-ZRS equation (11b) works at the small x range, for say $x < x_1$, where $x_1 = \mathcal{O}(10^{-1})$ according to $\alpha_s \ln(1/x)\ln(k_T^2/\mu^2) \sim \mathcal{O}(1)$. We take $x_1 = 0.15$ in this work.

Now we apply Eq. (21) in the nuclear target. Shadowing and antishadowing effects are thought to arise from a nonlinear mechanism which occurs when gluons are sufficiently dense to interact themselves. The strength of the gluon recombination is proportional to the gluon density on the transverse area. The gluons with smaller x exceed the longitudinal size of nucleon in a nucleus. Thus, the strength of the nonlinear recombination terms in Eq. (21) should be scaled by $A^{1/3}$ in a nucleus. On the other hand, although the softer gluons of different nucleons with extra small k_t maybe correlated on the transverse area because the integrations on k_t can go down to a very small value in Eq. (21), we neglect these corrections due to $F(x, k_t^2 \to 0) \to 0$. In this simple model, Eq. (21) in the nucleus becomes

$$-x\frac{\partial F_A(x,k_t^2)}{\partial x}$$

$$= \frac{\alpha_s N_c}{\pi}\int_{k^2_{1t,min}}^{k_t^2}\frac{dk^2_{1t}}{k^2_{1t}}F_A(x,k^2_{1t})$$

$$-A^{1/3}\frac{36\alpha_s^2}{\pi R^2 k_t^2}\frac{N_c^2}{N_c^2-1}\left[\int_{k^2_{1t,min}}^{k_t^2}\frac{dk^2_{1t}}{k^2_{1t}}F_A(x,k^2_{1t})\right]^2+A^{1/3}\frac{18\alpha_s^2}{\pi R^2 k_t^2}\frac{N_c^2}{N_c^2-1}\left[\int_{k^2_{1t,min}}^{k_t^2}\frac{dk^2_{1t}}{k^2_{1t}}F_A\left(\frac{x}{2},k^2_{1t}\right)\right]^2,$$

$$(10^{-2}\leq x\leq 0.15);$$

$$-x\frac{\partial F_A(x,k_t^2)}{\partial x}$$

$$= \frac{\alpha_s N_c}{\pi}\int_{k^2_{1t,min}}^{k_t^2}\frac{dk^2_{1t}}{k^2_{1t}}F_A(x,k^2_{1t})+A^{1/3}\frac{18\alpha_s^2}{\pi R^2 k_t^2}\frac{N_c^2}{N_c^2-1}\left[\int_{k^2_{1t,min}}^{k_t^2}\frac{dk^2_{1t}}{k^2_{1t}}F_A\left(\frac{x}{2},k^2_{1t}\right)\right]^2,\ (0.15\leq x\leq 0.3), \tag{22}$$

The input gluons distribute on the boundary line $(2x_0, k_t)$ at fixed $2x_0$. We take a larger value of x_0 as a starting point of the evolution, where the gluon fusion just begins and the nonlinear corrections to the input gluon distributions can be neglected. On the other hand, the contributions of the Fermi motion and nuclear binding effects to the nuclear parton distributions at small x are small. In this case, a nucleus is simply the incoherent sum of the constituent nucleons at $2x_0$ and we have

$$F(2x_0,k_t^2)=F_A(2x_0,k_t^2), \tag{23}$$

where the nuclear parton distributions have been normalized by derived A.

The DGLAP kernel in Eq. (21) resums the double leading $\alpha_s\ln(1/x)\ln(k_t^2/\mu^2)$ contributions. As we know that the BFKL evolution [23] which resums the leading $\ln(1/x)$ contributions and should completely replace the DGLAP equation at vary small x range, for say at $x<10^{-3}$ according to $\alpha_s\ln(1/x)\sim\mathcal{O}(1)$. In this regime, Eq. (2) is rewritten as

$$\Delta f(x,k_t^2)=\int_{k^2_{1t,min}}^{\infty}\frac{d^2\mathbf{k}_{1t}}{k^2_{1t}}\int_x^1\frac{dx_1}{x_1}\mathcal{K}\left(\frac{k_t^2}{k^2_{1t}},\frac{x}{x_1},\alpha_s\right)f(x_1,k^2_{1t}), \tag{24}$$

or

$$\Delta F(x,k_t^2)=\int_{k_{1t,min}^2}^{\infty}\frac{d^2\mathbf{k}_{1t}}{k_{1t}^2}\int_x^1\frac{dx_1}{x_1}\frac{x}{x_1}\mathcal{K}\left(\frac{k_t^2}{k_{1t}^2},\frac{x}{x_1},\alpha_s\right)F(x_1,k_{1t}^2), \tag{25}$$

where

$$F(x,k_t^2)=F(x_1,k_{1t}^2)+\Delta F(x,k_t^2), \tag{26}$$

and

$$\frac{x}{x_1}\mathcal{K}\left(\frac{k_t^2}{k_{1t}^2},\frac{x}{x_1},\alpha_s\right)\to\mathcal{K}_{BFKL}^{LL(1/x)}\left(\frac{k_t^2}{k_{1t}^2},\alpha_s\right). \tag{27}$$

In consequence, we have the linear BFKL equation (See Appendix B)

$$\begin{aligned}&-x\frac{\partial F(x,k_t^2)}{\partial x}\\&=\frac{\alpha_s N_c k_t^2}{\pi}\int_{k_{1t,min}^2}^{\infty}\frac{dk_{1t}^2}{k_{1t}^2}\left\{\frac{F(x,k_{1t}^2)-F(x,k_t^2)}{|k_{1t}^2-k_t^2|}+\frac{F(x,k_t^2)}{\sqrt{k_t^4+4k_{1t}^4}}\right\},\end{aligned} \tag{28}$$

and nonlinear BFKL equation with the modifications of gluon fusion

$$\begin{aligned}&-x\frac{\partial F(x,k_t^2)}{\partial x}\\&=\frac{\alpha_s N_c k_t^2}{\pi}\int_{k_{1t,min}^2}^{\infty}\frac{dk_{1t}^2}{k_{1t}^2}\left\{\frac{F(x,k_{1t}^2)-F(x,k_t^2)}{|k_{1t}^2-k_t^2|}+\frac{F(x,k_t^2)}{\sqrt{k_t^4+4k_{1t}^4}}\right\}\\&-\frac{36\alpha_s^2}{\pi R^2k_t^2}\frac{N_c^2}{N_c^2-1}\left[\int_{k_{1t,min}^2}^{k_t^2}\frac{dk_{1t}^2}{k_{1t}^2}F(x,k_{1t}^2)\right]^2+\frac{18\alpha_s^2}{\pi R^2k_t^2}\frac{N_c^2}{N_c^2-1}\left[\int_{k_{1t,min}^2}^{k_t^2}\frac{dk_{1t}^2}{k_{1t}^2}F\left(\frac{x}{2},k_{1t}^2\right)\right]^2;\end{aligned}$$

$$\begin{aligned}&-x\frac{\partial F_A(x,k_t^2)}{\partial x}\\&=\frac{\alpha_s N_c k_t^2}{\pi}\int_{k_{1t,min}^2}^{\infty}\frac{dk_{1t}^2}{k_{1t}^2}\left\{\frac{F_A(x,k_{1t}^2)-F_A(x,k_t^2)}{|k_{1t}^2-k_t^2|}+\frac{F_A(x,k_t^2)}{\sqrt{k_t^4+4k_{1t}^4}}\right\}\\&-A^{1/3}\frac{36\alpha_s^2}{\pi R^2k_t^2}\frac{N_c^2}{N_c^2-1}\left[\int_{k_{1t,min}^2}^{k_t^2}\frac{dk_{1t}^2}{k_{1t}^2}F_A(x,k_{1t}^2)\right]^2+A^{1/3}\frac{18\alpha_s^2}{\pi R^2k_t^2}\frac{N_c^2}{N_c^2-1}\left[\int_{k_{1t,min}^2}^{k_t^2}\frac{dk_{1t}^2}{k_{1t}^2}F_A\left(\frac{x}{2},k_{1t}^2\right)\right]^2.\end{aligned} \tag{29}$$

To make our progress we need to know how the BFKL formalism links with the conventional DGLAP dynamics. A usual framework which gives a unified treatment through out the (x, k_t) kinematic region has been provided by Catani, Ciafaloni, Fiorani and Marchesini (the CCFM equation [24]). This equation is based on the coherent radiation of gluons, which leads to an angular ordering of the gluon emissions along the chain. In the leading $\ln(1/x)$ approximation the CCFM equation reduces to the BFKL equation, whereas at moderate x the angular ordering becomes an ordering in the gluon transverse momenta and the CCFM equation becomes equivalent to standard DGLAP evolution.

Unfortunately, the CCFM schema contains the unknown shadowing and antishadowing information in its complicate input distributions. In this work we use following physical picture. As we know that the BFKL equation can be derived in a dipole picture (see Appendix B). At lager x region (for say, $x > 0.1$), parton densities in nucleon are dilute and the probe is interacted with a single parton (Fig.1 a). In this case, the DGLAP dynamics are dominated. On the other hand, at very small x region ($x < 10^{-3}$), the correlations among the initial partons in a nucleon becomes important and the dipole configuration dominates the initial state (Fig.1c), and the BFKL dynamics replace the DGLAP equation. Note that although $x < 10^{-3}$ is a dominated regime by the BFKL evolution according to $\alpha_s \ln(1/x) \sim \mathcal{O}(1)$, we can not exclude the BFKL dynamics participate the *part* of evolution at a more larger x region since $\alpha_s \ln(1/x) \ln(k_t^2/\mu^2) < 1$ allows $x > 10^{-3}$. Therefore, a natural connection between two evolution dynamics is that the BFKL dynamics replace asymptotically the DGLAP dynamics from $x = 0.1$ to 10^{-3} through the mixing of the single parton and dipole configuration as shown in Fig.1b. In the concretely, we take

$$Equation(21), \quad at \ 0.15 > x > 10^{-1};$$

$$Equation(21) \times [1-\beta] + Equatiuion(29) \times \beta, \ at \ 10^{-1} > x > 10^{-3};$$

$$Equation(29), \quad at \ x < 10^{-3}, \tag{30}$$

where

$$\beta = -\frac{\ln 10}{\ln 10^3 - \ln 10} + \frac{\ln \frac{1}{x}}{\ln 10^3 - \ln 10}. \tag{31}$$

We emphasize that if we use the original form of the GLR-MQ-ZRS equation (13) to replace Eq. (21), the solution of the Eq. (31) becomes very difficult since existing two different evolution ways.

All parameters in the solutions of Eqs. (21), (22) and (29) will be determined by the EMC effect. Most data about the EMC effect are measured by the structure functions. Thus, we should calculate the quark distributions at small x. We assume that the sea quark distributions at the small x range are dominated by the gluon distribution, via the DGLAP splitting $g \to q\overline{q}$. Thus, the deep inelastic structure function at small x reads [27]

$$F_2(x,Q^2)$$

$$= 2\int_x^1 dx_1 \int^{Q^2} \frac{dk_t^2}{k_t^2} \int^{k_t^2} \frac{dk_{1t}^2}{k_{1t}^2} F(\frac{x}{x_1}, k_{1t}^2) \sum_q e_q^2 \frac{\alpha_s}{2\pi} P_{qg}(x_1). \tag{32}$$

where $P_{qg}(x_1)$ is the DGLAP splitting function.

3 The EMC effect

We choose $x_0 = 0.15$ as the stating point of the evolution in Eqs. (21) and (22), where the nonlinear gluon recombination begins work. We find that following input is satisfy, i.e.,

$$F(2x_0, k_t^2) = 2\sqrt{(k_t^2)}exp(-(log(k_t^2))^2). \tag{33}$$

The computations of Eqs. (21), (22) and (29) need pre-know the value of $F(x_i/2, k_t^2)$ at the step $x = x_i$. For this sake, we proposed following program in [26]

$$F\left(\frac{x_i}{2}, k_t^2\right) = F_{Shadowing}\left(\frac{x_i}{2}, k_t^2\right) + \frac{F_{linear}\left(\frac{x_i}{2}, k_t^2\right) - F_{Shadowing}\left(\frac{x_i}{2}, k_t^2\right)}{i\Delta - \Delta + 1}, \tag{34}$$

where $F_{Shadowing}(x_i/2, k_t^2)$ (or $F_{linear}(x_i/2, k_t^2)$) indicates that the evolution from x_i to $x_i/2$ is controlled by Eqs. (21), (22) and (29) but without the antishadowing contributions (or is controlled by the linear equation). The parameter $0 < \Delta < 1$ implies the different velocities approaching to the dynamics of Eqs. (21), (22) and (29).

At first, we use the well known $F_{2p}(x, Q^2)$-data [25] of a free proton to determine the parameters in the computations. Then we predict the distributions in nuclei. The dashed curve in Fig. 2 is our fitting result using the input (33), where we take the parameters $R = 2.4\ GeV^{-1}$, $k_t^2 = 0.01 GeV^2$, $\alpha_s = 0.3$ and $\Delta = 0.02$. Note that the contributions from the valence quarks to F_2 at $x > 0.1$ are necessary and they can be parameterized by the difference between the dashed curve and experimental solid curve in Fig.2.

Figure 3 shows our predictions of Eqs. (21), (22) and (29) for the Ca/C, C/Li, Ca/D and Cu/D compared with the EMC and NMC results [28,29]. The agreement is acceptable.

It is different from the scheme of the DGLAP evolution equation, we can predict the nuclear effects for the unintegrated gluon distribution. The results are presented by the

ratios of the nuclear unintegrated gluon distributions in Figs.4 and 5. Although deep inelastic scattering experiments do not provide the direct test of these effects, hadron-nucleus scattering at RHIC relates to the nuclear unintegrated gluon distributions and we will use them in next section.

The ratios $G_{Ca}(x,Q^2)/G_D(x,Q^2)$ for gluon distributions at $Q^2 = 2$ and 10 GeV^2 using Eqs. (21), (22) and (29) are given in Fig.6. The Q^2-dependence of the gluon ratio is predicted in the region $10^{-4} < x < 10^{-1}$ in our model. The logarithmic slope b in $G_A/G_{A'} = a + b\ln Q^2$ is positive. However, the corresponding slope in the ratio of the structure functions F_{2Ca}/F_{2D} is negative at small x (see Fig.7). For example, the predicted Q^2-slope for calcium at $x \simeq 4\times 10^{-2}$, $b \simeq -0.046$, and at $x \simeq 10^{-2}$, $b \simeq -0.03$, the results are compatible with the measured data in [30].

The data of $G_{Sn}(x,Q^2)/G_C(x,Q^2)$ are measured from inelastic J/ψ production by the NM Collaboration in Ref. [31], which determine a stronger nuclear antishadowing effect but with a larger uncertainty. Our prediction is presented in Fig.8.

Comparing with the ESP09 set [13], we predict a more stronger antishadowing effect in the gluon (integrated and unintegrated) distributions of heavy nucleus. One of the reasons is that the observed antishadowing effect in the structure functions origins dynamically from the gluon fusions in our model, while in the DGLAP analysis it is partly from the input distributions of the valence quarks [13]. The second reason is that the A-dependent nonlinear terms enhance the effect of the gluon fusion in the heavy nuclei.

4 The Cronin effect

The Cronin effect is described by the nuclear modification factor R_{dA}, which is defined as the ratio of the number of particles produced in a $d+A$ collision over the number of particles produced in a $p+p$ collision scaled by the number of collisions

$$R_{dA}(k_t) = \left. \frac{\frac{dN_{d-A}(k_t,\eta)}{d^2k_T d\eta}}{N_{coll}\frac{dN_{p-p}(k_t,\eta)}{d^2k_t d\eta}} \right|_{\eta=0}, \tag{35}$$

k_t and η are the transverse momentum and the pseudo-rapidity of the observed hadron, respectively. N_{coll} is the number of collisions in $d+A$ scattering. In Eq. (35),

$$\frac{dN_{p-p}(k_t,\eta)}{d^2k_t d\eta} = \frac{1}{\sigma_{in}}\frac{d\sigma_{p-p}(k_t,\eta)}{d^2k_t d\eta}$$
$$= \frac{1}{\sigma_{in}}\int \frac{dz}{z} J(\eta; k_t; m_{eff})\ D_p(z)\delta^2(k_t - zk_{t,g})\left.\frac{d\sigma_{p-p}(k_{t,g},y)}{dyd^2k_{t,g}}\right|_{y\to\eta}, \tag{36}$$

and

$$\frac{1}{N_{coll}}\frac{dN_{d-A}}{d^2k_t d\eta} = \frac{1}{\sigma_{in}}\frac{d\sigma_{d-A}(k_t,\eta)}{d^2k_t d\eta}$$
$$= \frac{1}{\sigma_{in}}\int \frac{dz}{z} J(\eta; k_t; m_{eff})\ D_A(z)\delta^2(k_t - zk_{t,g})\left.\frac{d\sigma_{d-A}(k_{t,g},y)}{dyd^2k_{t,g}}\right|_{y\to\eta}, \tag{37}$$

where $z = k_t/k_{t,g}$; $D_p(z)$ and $D_A(z)$ are the fragmentation functions of gluon jets in proton and nucleus, where the factorized scale-dependence of the fragmentation functions are neglected; The rapidity y of the produced gluon in the center-of-mass frame of $p+p$ collisions is defined by

$$x_{1/2} = \frac{k_{t,g}}{\sqrt{s}} \cdot \exp(\pm y); \tag{38}$$

The relation between the rapidity y and pseudorapidity η for massive particles is

$$y = \frac{1}{2}\ln\left[\frac{\sqrt{\frac{m_{eff}^2+p_t^2}{p_t^2}+\sinh^2\eta}+\sinh\eta}{\sqrt{\frac{m_{eff}^2+p_t^2}{p_t^2}+\sinh^2\eta}-\sinh\eta}\right], \tag{39}$$

where m_{eff} is the typical invariant mass of the gluon jet.

We assume that the hadrons in the central region are produced from the hadronization of the gluons in $gg \to g$ mechanism. According to Ref. [16] we have

$$\begin{aligned}
&\left.\frac{d\sigma_{p-p}(k_t,\eta)}{d^2k_t d\eta}\right|_{\eta=0} \\
&= \frac{4N_c}{N_c^2-1}\int\frac{dz}{z^2}\frac{\alpha_s}{k_{t,g}^2}J^2 D_p(z) \\
&\int^{k_{t,g}^2} dq_{t,g}^2 \varphi_g^p(x,(k_{t,g}-q_{t,g})^2)\varphi_g^p(x,q_{t,g}^2)\Big|_{k_{t,g}=Jk_t/z} \\
&\simeq \frac{4N_c}{N_c^2-1}\int\frac{dz}{z^2}\frac{\alpha_s}{k_{t,g}^2}J^2 D_p(z) \\
&\left[\varphi_g^p(x,k_{t,g}^2)G^p(x,k_{t,g}^2)+G^p(x,k_{t,g}^2)\varphi_g^p(x,k_{t,g}^2)\right]_{k_{t,g}=Jk_t/z},
\end{aligned} \tag{40}$$

$$\begin{aligned}
&\left.\frac{d\sigma_{d-A}(k_t,\eta)}{d^2k_t d\eta}\right|_{\eta=0} \\
&= \frac{4N_c}{N_c^2-1}\int\frac{dz}{z^2}\frac{\alpha_s}{k_{t,g}^2}J^2 D_A(z) \\
&\int^{k_{t,g}^2} dq_{t,g}^2 \varphi_g^p(x,(k_{t,g}-q_{t,g})^2)\varphi_g^A(x,q_{t,g}^2)\Big|_{k_{t,g}=Jk_t/z} \\
&\simeq \frac{4N_c}{N_c^2-1}\int\frac{dz}{z^2}\frac{\alpha_s}{k_{t,g}^2}J^2 D_A(z) \\
&\left[\varphi_g^p(x,k_{t,g}^2)G^A(x,k_{t,g}^2)+G^p(x,k_{t,g}^2)\varphi_g^A(x,k_{t,g}^2)\right]_{k_{t,g}=Jk_t/z},
\end{aligned} \tag{41}$$

where $\varphi_g(x,q_{t,g}^2) = F(x,q_{t,g}^2)/q_{t,g}^2$ and we neglect the k_t-dependence in the fragmentation functions.

At first step, we neglect the interactions at final state, i.e., in Eqs. (40) and (41)

$$D_p(z) = D_A(z) = \delta(z-1). \tag{42}$$

We indicate this nuclear modification factor as R^g_{dA}, which is drawn in Fig. 9. According to Eq. (38) at $y = 0$ and $\sqrt{s} = 200GeV$, the antishadowing effect on the gluon jet should distribute in a broad range $8GeV < k_t < 60GeV$, which corresponds to the antishadowing range $0.02 < x < 0.3$ in Fig.4.

In next step, we consider the corrections from the fragmentation functions but neglecting the difference between proton and nucleus. We take [32]

$$D_p(z) = D_A(z) = \frac{2}{3} \times 1940 z^{1.4}(1-z)^8, \tag{43}$$

where $D(z) \to 0$ at $z \to 0$ since the coherence effects in QCD at small z. Our results are plotted by the solid curve in Fig. 10. The data are taken from the BRAHMS results in [6]. One can find that the fragmentation functions shift cross point between the Cronin and anti-Cronin effects toward to small k_t, since the position of the peak value of the fragmentation functions always localizes at small z. We find that the nuclear shadowing and antishadowing effects at the initial state dominate the Cronin effect, although a small nuclear modification to the fragmentation functions, i.e., $D_A(z) \neq D_p(z)$ is necessary.

The parton energy loss caused by medium-induced multiple gluon emission in various nuclear conditions is a hot topic, since the data in the RHIC $Au+Au$ collisions show a new hot matter and it is maybe a strongly coupled Quark-Gluon Plasma (sQGP). The presence of a dense medium influences the space-time development of the partonic shower of a jet. An energetic jet parton propagates through the medium, a part of its energy transfers to the thermal partons, and it is called the parton energy loss. After this jet propagates a longer distance in an expanding de-confinement system, most gluons carrying the lost energy escape from the jet cone, and they are un-measured. Thus, for an example, the modified fragmentation function in an effective model can be written as [33]

$$D_A(z) = \frac{1}{1-\epsilon} D_p(\frac{z}{1-\epsilon}), \tag{44}$$

where E is the initial energy of a gluon jet and $\epsilon = \Delta E/E$ is fractional energy loss.

We consider that a similar energy loss mechanism also exits in the RHIC $d + Au$ collisions but with a smaller value of ϵ. The dashed curve in Fig. 10 is the resulting nuclear suppression factor with $\epsilon = 0.1$. From the above mentioned results we find that the anti-Cronin suppression and Cronin enhancement origin from the nuclear shadowing and antishadowing effects in the initial state as in the EMC effect.

Using the above mentioned parameters we predict the Cronin effect in $d+Pb$ collisions at the CERN Large Hadron Collider (LHC). The results in Fig. 11 show that the anti-Cronin suppression dominates a broad k_t range, while the Cronin enhancement appears at large k_t range. This character is different from the RHIC data and it comes from the kinematical x range. The value of x in LHC is much small, where the nuclear shadowing dominates the gluon distribution. While the value of x in RHIC can reach the nuclear antishadowing range.

5 The signals of QGP

One of the important findings at RHIC and LHC is that high transverse momentum hadron production in central heavy ion collisions is suppressed compared to (properly scaled) p+p collisions [1, 2], which is defined as the nuclear suppression factor R_{AA}. This suppression can be attributed to energy loss of high-k_t partons that traverse the hot and dense medium formed in these collisions. However, the extraction of the energy loss from R_{AA} needs to know the nuclear effects in the initial parton distributions. Our obtained integrated and unintegrated gluon distributions in proton and nuclei provide such information.

Some of the most important results obtained at RHIC are related with the high-k_t spectrum in heavy ion $Au + Au$ collisions. In this aspect, a precise determination of the nuclear effects in the initial state of the collision is fundamental. In what follows we present the estimation for the ratio R_{AA}

$$R_{AA}(k_t) = \left. \frac{\frac{dN_{A-A}(k_t,\eta)}{d^2k_T d\eta}}{N_{coll}\frac{dN_{p-p}(k_t,\eta)}{d^2k_t d\eta}} \right|_{\eta=0}, \tag{45}$$

using our parameters in the explanation of the EMC- and Cronin-effects. At first step, we assume that $\epsilon = 0$ in Eq. (44) and show the nuclear shadowing and antishadowing effects in the nuclear suppression factor. The result is dashed curve in Fig. 12. One can find that a big difference between dashed curve and data at $k_t > 5GeV$, which is commonly interpreted in terms of a strong energy loss of the energetic partons when traversing a dense medium. For example, we take $\epsilon = 0.4$ and the result is the pointed curve in Fig. 12. Obviously, a true form of fractional energy loss ϵ is crossover from the smaller value of ϵ the larger one when increasing energy of the gluon jet. It is interest that we take

$$\epsilon = \begin{cases} a & \text{if } E < E_c \\ b & \text{if } E > E_c \end{cases}, \tag{46}$$

where $a = 0.2$ and $b = 0.4$ (i.e., Fig. 13a); similar to Eq. (41) we have

$$\left.\frac{d\sigma_{A-A}(k_t,\eta)}{d^2k_t d\eta}\right|_{\eta=0}$$

$$= \frac{4N_c}{N_c^2-1}\int_0^{k_t/E_c}\frac{dz}{z^2}\frac{\alpha_s}{k_{t,g}^2}J^2 D_A(z)\left[\varphi_g^A(x,k_{t,g}^2)G^A(x,k_{t,g}^2)+G^A(x,k_{t,g}^2)\varphi_g^A(x,k_{t,g}^2)\right]_{k_{t,g}=Jk_t/z}$$

$$+\frac{4N_c}{N_c^2-1}\int_{k_t/E_c}^{1-a}\frac{dz}{z^2}\frac{\alpha_s}{k_{t,g}^2}J^2 D_A(z)\left[\varphi_g^A(x,k_{t,g}^2)G^A(x,k_{t,g}^2)+G^A(x,k_{t,g}^2)\varphi_g^A(x,k_{t,g}^2)\right]_{k_{t,g}=Jk_t/z}$$

$$if\ k_t < E_c(1-b);$$

$$= \frac{4N_c}{N_c^2-1}\int_0^{1-b}\frac{dz}{z^2}\frac{\alpha_s}{k_{t,g}^2}J^2 D_A(z)\left[\varphi_g^A(x,k_{t,g}^2)G^A(x,k_{t,g}^2)+G^A(x,k_{t,g}^2)\varphi_g^A(x,k_{t,g}^2)\right]_{k_{t,g}=Jk_t/z}$$

$$+\frac{4N_c}{N_c^2-1}\int_{k_t/E_c}^{1-a}\frac{dz}{z^2}\frac{\alpha_s}{k_{t,g}^2}J^2 D_A(z)\left[\varphi_g^A(x,k_{t,g}^2)G^A(x,k_{t,g}^2)+G^A(x,k_{t,g}^2)\varphi_g^A(x,k_{t,g}^2)\right]_{k_{t,g}=Jk_t/z}$$

$$if\ E_c(1-b) < k_t < E_c(1-a);$$

$$= \frac{4N_c}{N_c^2-1}\int_0^{1-b}\frac{dz}{z^2}\frac{\alpha_s}{k_{t,g}^2}J^2 D_A(z)\left[\varphi_g^A(x,k_{t,g}^2)G^A(x,k_{t,g}^2)+G^A(x,k_{t,g}^2)\varphi_g^A(x,k_{t,g}^2)\right]_{k_{t,g}=Jk_t/z}$$

$$if\ k_t > E_c(1-a), \tag{47}$$

we find that the resulting (solid curve) in Fig. 12 perfect to fit the data at $1GeV < k_t < 10GeV$.

Recently, the nuclear modification factor in central Pb+Pb collisions at $\sqrt{s} = 2.76TeV$ is published by the ALICE Collaboration at the LHC [2]. The data indicate that R_{AA} reaches a minimum of about 0.14 at $k_t = 6-7GeV$, which is smaller than at RHIC, however, it steeply rises over the asymptotic value of RHIC at larger k_t. Therefore, it is unclear whether a more denser mater is formed at LHC. Obviously, a quantitative determination of the energy loss excluding gluon shadowing and antishadowing effects is necessary. For this sake, similar to the above mentioned approach in the RHIC data, we take $a = 0$ and $b = 0.58$ (Fig. 13b) in Eq. (46) and the result is presented the solid curve

in Fig. 14. The dashed and pointed curves correspond to $\epsilon = 0$ and 0.58, respectively. Although the data show that the energy loss ϵ will decrease with the jet energy $E >> 10\ GeV$, Eq. (46) is a good approximation describing the nuclear suppression factor at $1GeV < k_t < 10GeV$. Thus, we find a rapid crossover from week energy loss to strong energy loss at a universal critical energy of gluon jet $E_c \sim 10GeV$. Using same parameters we predict the nuclear suppression factor in central $Pb + Pb$ collisions at $\sqrt{s} = 5.5$ and $7.7TeV$ in Figs. 15 and 16.

In summary, the EMC- and Cronin-effects are explained by a unitarized evolution equation, where the shadowing and antishadowing corrections are dynamically produced by gluon fusions. For this sake, an alternative form of the GLR-MQ-ZRS equation is derived. The resulting integrated and unintegrated gluon distributions in proton and nuclei are used to analyze the contributions of the initial parton distributions to the nuclear suppression factor in heavy ion collisions. A simulation of the fractional energy loss is extracted from the RHIC and LHC data, where the contributions of the nuclear shadowing and antishadowing effects are considered. We find a rapid crossover from week energy loss to strong energy loss at a universal critical energy of gluon jet $E_c \sim 10GeV$.

Acknowledgments: This work was supported in part by the National Natural Science Foundations of China 10875044 and the Project of Knowledge Innovation Program (PKIP) of Chinese Academy of Sciences, Grant No. KJCX2.YW.W10

Appendix A. GLR-MQ-ZRS equation: The modifications of the gluon recombination to the DGLAP evolution in the GLR-MQ-ZRS equation has following form [19,20].

$$\frac{dG(x,Q^2)}{d\ln Q^2}$$

$$= P_{gg}^{AP} \otimes G(x,Q^2) + P_{gq}^{AP} \otimes S(x,Q^2)$$

$$-2\int_x^{1/2} \frac{dx_1}{x_1}\frac{x}{x_1}\mathcal{K}_{GLR-MQ-ZRS}^{GG\to GG,\ LL(Q^2)}\left(\frac{x}{x_1},\alpha_s\right) G^{(2)}(x_1,\mu_1^2)$$

$$+\int_{x/2}^{1/2} \frac{dx_1}{x_1}\frac{x}{x_1}\mathcal{K}_{GLR-MQ-ZRS}^{GG\to GG,\ LL(Q^2)}\left(\frac{x}{x_1},\alpha_s\right) G^{(2)}(x_1,\mu_1^2), \qquad (A-1)$$

for gluon distribution and

$$\frac{dxS(x,Q^2)}{d\ln Q^2}$$

$$= P_{qg}^{AP} \otimes G(x,Q^2) + P_{qq}^{AP} \otimes S(x,Q^2)$$

$$-2\int_x^{1/2} \frac{dx_1}{x_1}\frac{x}{x_1}\mathcal{K}_{GLR-MQ-ZRS}^{GG\to S\overline{S},\ LL(Q^2),}\left(\frac{x}{x_1},\alpha_s\right) G^{(2)}(x_1,\mu_1^2)$$

$$+\int_{x/2}^{1/2} \frac{dx_1}{x_1}\frac{x}{x_1}\mathcal{K}_{GLR-MQ-ZRS}^{GG\to S\overline{S},\ LL(Q^2)}\left(\frac{x}{x_1},\alpha_s\right) G^{(2)}(x_1,\mu_1^2), \qquad (A-2)$$

for sea quark distributions, where P^{AP} are the evolution kernels of the linear DGLAP equation and the recombination functions

$$\frac{dx_1}{x_1}\mathcal{K}_{GLR-MQ-ZRS}^{GG\to GG,\ LL(Q^2)}$$

$$= \frac{9\alpha_s^2}{64}\frac{(2x_1-x)(72x_1^4-48x_1^3x+140x_1^2x^2-116x_1x^3+29x^4)}{x_1^5x}dx_1 \qquad (A-3)$$

$$\frac{dx_1}{x_1}\mathcal{K}_{GLR-MQ-ZRS}^{GG\to S\overline{S},\ LL(Q^2)}$$

$$= \frac{\alpha_s^2}{48}\frac{(2x_1-x)^2(18x_1^2-21x_1x+14x)}{x_1^5}dx_1 \qquad (A-4)$$

Appendix B. A derivation of the BFKL equation in the dipole picture:

In order to certify the physical picture in Fig. 1, we give a derivation of the BFKL equation in the dipole picture. We consider the DIS process in Fig. 17, where the dashed lines are the time-ordering lines in the TOPT. These processes imply a scattered gluon before its radiation is omitted from two correlating gluons. We call such a correlating gluon cluster as a dipole, which phenomenologically describes the correlation among initial partons.

The evolution kernel in a QCD evolution equation is a part of more complicated scattering diagram. In general, the correlations among the initial partons make these partons off mass-shell. One of the most important hypotheses in the derivation of the DGLAP equation is that all correlations among initial partons are negligible during the interaction. Therefore, the interaction of a virtual probe with the nucleon can be factorized as the nonperturbative parton distribution and hard probe-parton matrix in the collinear factorization scheme. At the higher density range of partons, these correlations among the initial partons can no longer be neglected. In this case, the transverse momenta of the initial partons are non-zero and these partons are generally off mass-shell, therefore, the k_T-factorization scheme is necessary.

In this work we use the semi-classical Weizsäcker-Williams ($W-W$) approximation [34] to realize the k_t-factorization scheme. The reason is that the $W-W$ approximation allows us to extract the evolution kernels and to keep all initial and final partons of the evolution kernels on their mass-shell.

For convenience, we use $\underline{k}$ to indicate the transverse momentum k_t in this section. We consider that the observed wave function $\Psi(x_2,\underline{k})$ is evolved from the initial wave functions $\Psi(x_1,\underline{p}_a)$ and $\Psi(x_1,\underline{p}_b)$ via the QCD interactions, i.e.,

$$\Psi(x_2,\underline{k}) = \Psi(x_1,\underline{p}_a)A_{BFKL1} + \Psi(x_1,\underline{p}_b)A_{BFKL2}, \qquad (B-1)$$

where two perturbative amplitudes corresponding to Fig. 17 are

$$A_{BFKL1} = \sqrt{\frac{2E_k}{E_{p_a}+E_{p_b}}}\frac{1}{2E_k}\frac{1}{E_k+E_{l_a}-E_{p_a}}M_1, \qquad (B-2)$$

and

$$A_{BFKL2} = \sqrt{\frac{2E_k}{E_{p_a}+E_{p_b}}}\frac{1}{2E_k}\frac{1}{E_k+E_{l_b}-E_{p_b}}M_2. \qquad (B-3)$$

The momenta of the partons are parameterized as

$$p_a = (x_1P + \frac{(\underline{k}+\underline{l}_a)^2}{2x_1P}, \underline{k}+\underline{l}_a, x_1P), \qquad (B-4)$$

$$k = (x_2P + \frac{\underline{k}^2}{2x_2P}, \underline{k}, x_2P), \qquad (B-5)$$

$$l_a = ((x_1-x_2)P + \frac{\underline{l}_a^2}{2(x_1-x_2)P}, \underline{l}_a, (x_1-x_2)P), \qquad (B-6)$$

$$p_b = (x_1P + \frac{(\underline{k}+\underline{l}_b)^2}{2x_1P}, \underline{k}+\underline{l}_b, x_1P), \qquad (B-7)$$

and

$$l_b = ((x_1-x_2)P + \frac{\underline{l}_b^2}{2(x_1-x_2)P}, \underline{l}_b, (x_1-x_2)P). \qquad (B-8)$$

The matrixes of the local QCD interactions are

$$M_1 = igf^{abc}[g_{\alpha\beta}(p_a+k)_\gamma + g_{\beta\gamma}(-k+l_a)_\alpha + g_{\gamma\alpha}(-l_a-p_a)_\beta]\epsilon_\alpha(p_a)\epsilon_\beta(k)\epsilon_\gamma(l_a), \quad (B-9)$$

$$M_2 = igf^{abc}[g_{\alpha\beta}(p_b+k)_\gamma + g_{\beta\gamma}(-k+l_b)_\alpha + g_{\gamma\alpha}(-l_b-p_b)_\beta]\epsilon_\alpha(p_b)\epsilon_\beta(k)\epsilon_\gamma(l_b), \quad (B-10)$$

where the polarization vectors are

$$\epsilon(p_a) = (0, \underline{\epsilon}, -\frac{\underline{\epsilon}\cdot(\underline{k}+\underline{l}_a)}{x_1 P}), \quad (B-11)$$

$$\epsilon(k) = (0, \underline{\epsilon}, -\frac{\underline{\epsilon}\cdot\underline{k}}{x_2 P}), \quad (B-12)$$

and

$$\epsilon(l_a) = (0, \underline{\epsilon}, -\frac{\underline{\epsilon}\cdot\underline{l}_a}{(x_1-x_2)P}), \quad (B-13)$$

where $\underline{\epsilon}$ is the transverse polarization of the gluon in $\epsilon_\mu = (\epsilon_0, \underline{\epsilon}, \epsilon_3) = (0, \underline{\epsilon}, 0)$, since the sum includes only physical transverse gluon states in the TOPT form [19].

Taking the LL(1/x) approximation, i.e., assuming that $x_2 \ll x_1$, one can get two similar amplitudes

$$A_{BFKL1} = igf^{abc}2\sqrt{\frac{x_1}{x_2}}\frac{\underline{\epsilon}\cdot\underline{k}}{\underline{k}^2}, \quad (B-14)$$

and

$$A_{BFKL2} = igf^{abc}2\sqrt{\frac{x_1}{x_2}}\frac{\underline{\epsilon}\cdot\underline{k}}{\underline{k}^2}. \quad (B-15)$$

However, these two amplitudes really occupy different transverse configurations. This is a reason why the dipole model of the BFKL equation is derived by using the transverse coordinator-space. However, we shall show that the momentum representation still can be used to distinguish the differences between Eqs. (B-14) and (B-15).

The two parton correlation function is generally defined as

$$|\Psi(x,\underline{p}_a,\underline{p}_b)|^2 = f(x,\underline{p}_a,\underline{p}_b)$$
$$= f\left(x,\frac{\underline{p}_a+\underline{p}_b}{2},\underline{p}_a-\underline{p}_b\right) \equiv f(x,\underline{k}_c,\underline{k}_{ab}), \qquad (B-16)$$

where $\underline{k}_c$ and $\underline{k}_{ab}$ are conjugate to the impact parameter and transverse scale of a cold spot. Equation (B-16) implies the probability finding a gluon, which carries the longitudinal momentum fraction x of a nucleon and locals inside a dipole characterizing by $\underline{k}_c$ and $\underline{k}_{ab}$.

In this work we derive the evolution equations in the impact parameter-independent case. This approximation implies that the evolution dynamics of the partons are dominated by the internal structure of dipole. Thus, the evolution kernel is irrelevant to $\underline{k}_c$ and we shall use

$$f(x,\underline{k}_{ab}) = \int \frac{d^2\underline{k}_c}{\underline{k}_c^2} f(x,\underline{k}_c,\underline{k}_{ab}), \qquad (B-17)$$

which has the following TOPT-structure

$$f(x,\underline{k}_{ab})$$
$$\equiv \frac{E_{ab}}{2E_P}|M_{P\to k_{ab}X}|^2\left[\frac{1}{E_P-E_{ab}-E_X}\right]^2\left[\frac{1}{2E_{ab}}\right]^2\prod_X \frac{d^3k_X}{(2\pi)^3 2E_X}. \qquad (B-18)$$

Notice that all transverse momenta in Eqs. (B-1)-(B-15) are indicated relative to the mass-center of the nucleon target. However according to Eq. (B-17), the evolution variable is the relative momentum $\underline{k}_{ab}$, therefore, it is suitable to rewrite all momenta to relative to $\underline{p}_b$ in Eq. (B-2) and to $\underline{p}_a$ in Eq. (B-3), respectively. Thus, we replace the transverse momenta as follows:

$$\underline{p}_a \to \underline{p}_a - \underline{p}_b \equiv \underline{k}_{ab},$$

$$\underline{k} \to \underline{k} - \underline{p}_b \equiv \underline{k}_{0b},$$

and

$$\underline{l}_a \to \underline{k}_{ab} - \underline{k}_{0b} = \underline{p}_a - \underline{k}_t \equiv \underline{k}_{a0}, \qquad (B-19)$$

in Eq. (2.6) since

$$\underline{k}_{ab} = \underline{k}_{a0} + \underline{k}_{0b}, \qquad (B-20)$$

and

$$\underline{p}_b \to \underline{p}_b - \underline{p}_a = \underline{k}_{ba},$$

$$\underline{k} \to \underline{k} - \underline{p}_a \equiv \underline{k}_{0a},$$

and

$$\underline{l}_b \to \underline{k}_{ba} - \underline{k}_{0a} = \underline{p}_b - \underline{k} = \underline{k}_{b0}, \qquad (B-21)$$

in Eq. (B-3). In consequence, we have

$$\Psi(x_1, \underline{p}_a) = \Psi(x_1, \underline{p}_b) = \Psi(x_1, \underline{k}_{ab}), \qquad (B-22)$$

and

$$A_{BFKL}(\underline{k}_{a0}, \underline{k}_{0b}, x_1, x_2) = igf^{abc} 2\sqrt{\frac{x_1}{x_2}} \left[\frac{\underline{k}_{a0}}{\underline{k}_{a0}^2} + \frac{\underline{k}_{0b}}{\underline{k}_{0b}^2} \right] \cdot \underline{\epsilon}, \qquad (B-23)$$

where we identify two $\underline{\epsilon}$ in Eq. (B-23) since the measurements on $(x_2, \underline{k}_{a0}^2)$ and $(x_2, \underline{k}_{0b}^2)$ are really the same event.

Equation (B-1) with Eqs. (B-22) and (B-23) provide such a picture: a parent dipole with the longitudinal momentum fraction x_1 and transverse momentum $\underline{k}_{ab}$ radiates a gluon, which has the longitudinal momentum fraction x_2 and the transverse momentum $\underline{k}_{a0}$ (or $\underline{k}_{0b}$).

We take the square of the total amplitude, one can get

$$
\begin{aligned}
& d\sigma(q_{probe}P \to k'X) \\
&= \frac{E_{ab}}{2E_P}|M_{P\to k_{ab}X}|^2 \left[\frac{1}{E_P - E_{ab} - E_X}\right]^2 \left[\frac{1}{2E_{ab}}\right]^2 \prod_X \frac{d^3k_X}{(2\pi)^3 2E_X} \\
&\quad \times \sum_{pol} A_{BFKL} A^*_{BFKL} \frac{d^3k_{ab}}{(2\pi)^3 E_{ab}} \\
&\quad \times \frac{1}{8E_k E_{probe}} |M_{q_{probe}k\to k'}|^2 (2\pi)^4 \delta^4(q_{probe} + k - k') \frac{d^2k'}{(2\pi)^3 2E_{k'}} \\
&= f(x_1, \underline{k}_{ab}) \otimes \frac{x_1}{x_2} \mathcal{K}_{BFKL}\left(\underline{k}_{ab}, \underline{k}_{a0}, \alpha_s\right) \otimes d\sigma(q^*_{probe} k(x_2, \underline{k}_{a0}) \to k'(x_2, \underline{k}')) \\
&\equiv \Delta[\Psi(x_2, \underline{k}_{a0})\Psi^*(x_2, \underline{k}_{a0}) + \Psi(x_2, \underline{k}_{a0})\Psi^*(x_2, \underline{k}_{0b}) + \\
&\Psi(x_2, \underline{k}_{0b})\Psi^*(x_2, \underline{k}_{a0}) + \Psi(x_2, \underline{k}_{0b})\Psi^*(x_2, \underline{k}_{0b})] \otimes d\sigma(q^*_{probe} k(x_2, \underline{k}_{a0}) \to k'(x'_2, \underline{k}')) \\
&= \Delta f(x_2, \underline{k}_{a0}) \otimes d\sigma(q^*_{probe} k(x_2, \underline{k}_{a0}) \to k'(x_2, \underline{k}')), \qquad (B-24)
\end{aligned}
$$

where on the last step, because the probe only picks up the contributions from $\Psi(x_2, \underline{k}_{a0})\Psi^*(x_2, \underline{k}_{a0})$, we regard $\Delta f(x_2, \underline{k}_{a0})$ as the increment of the distribution $f(x_1, \underline{k}_{ab})$ when it evolves from $(x_1, \underline{k}_{ab})$ to $(x_2, \underline{k}_{a0})$. Therefore we have

$$
\begin{aligned}
& \Delta f(x_2, \underline{k}_{a0}) \\
&= \int \frac{d\underline{k}_{ab}}{\underline{k}^2_{ab}} \int_{x_2}^1 \frac{dx_1}{x_1} \frac{x_1}{x_2} \mathcal{K}_{BFKL}\left(\underline{k}_{ab}, \underline{k}_{a0}, \alpha_s\right) f(x_1, \underline{k}_{ab}), \qquad (B-25)
\end{aligned}
$$

or

$$
\begin{aligned}
& \Delta\tilde{F}(x_2, \underline{k}_{a0}) \equiv \Delta x_2 f(x_2, \underline{k}_{a0}) \\
&= \int \frac{d\underline{k}^2_{ab}}{\underline{k}^2_{ab}} \int_{x_2}^1 \frac{dx_1}{x_1} \mathcal{K}_{BFKL}\left(\underline{k}_{ab}, \underline{k}_{a0}, \alpha_s\right) \tilde{F}(x_1, \underline{k}_{ab}). \qquad (B-26)
\end{aligned}
$$

Using definition

$$
\tilde{F}(x_2, \underline{k}_{a0}) = \tilde{F}(x_1, \underline{k}_{ab}) + \Delta\tilde{F}(x_2, \underline{k}_{a0}), \qquad (B-27)
$$

we write

$$-x\frac{\partial\tilde{F}(x,\underline{k}_{a0})}{\partial x}$$
$$=\int d\underline{k}^2_{ab}\mathcal{K}_{BFKL}(\underline{k}_{ab},\underline{k}_{a0},\alpha_s)\tilde{F}(x,\underline{k}_{ab}), \qquad (B-28)$$

According to Eq. (B-22), the evolution kernel reads as

$$\mathcal{K}_{BFKL}(\underline{k}_{ab},\underline{k}_{a0},\alpha_s)\frac{x_1}{x_2}\frac{dx_1}{x_1}d^2\underline{k}_{ab}=\sum_{pol}A_{BFKL}A^*_{BFKL}\frac{dx_1}{2x_1}\frac{d^2\underline{k}_{ab}}{(2\pi)^3}$$
$$=\frac{\alpha_s N_c}{\pi^2}\frac{\underline{k}^2_{ab}}{\underline{k}^2_{a0}\underline{k}^2_{0b}}\frac{dx_1}{x_2}d^2\underline{k}_{ab}. \qquad (B-29)$$

Finally Eq. (B-28) becomes

$$-x\frac{\partial\tilde{F}(x,\underline{k}_{a0})}{\partial x}$$
$$=\frac{\alpha_s N_c}{\pi^2}\int d^2\underline{k}_{ab}\frac{\underline{k}^2_{ab}}{\underline{k}^2_{a0}\underline{k}^2_{0b}}\tilde{F}(x,\underline{k}_{ab}). \qquad (B-30)$$

This is the real part of the BFKL equation.

Using the TOPT-cutting rules [19], one can prove that the virtual diagrams in Fig. 17 contribute the similar evolution kernel as the real kernel but differ by a factor $-1/2\times(1/2+1/2)$. Here we call the cut diagram with a naive partonic amplitude without any QCD-corrections as the virtual diagram. The negative sign arises from the changes of time order in the energy denominators. The factor $(1/2+1/2)$ is due to the fact that the probe "sees" only the square root of the parton distribution accepting the contributions of the partonic processes in a virtual diagram, and the other factor $1/2$ origins from the symmetry of the pure gluon process. Therefore, the evolution equation corresponding to Fig. 17 is

$$-x\frac{\partial\tilde{F}(x,\underline{k}_{ab})}{\partial x}$$

$$= -\frac{1}{2}\frac{\alpha_s N_c}{\pi^2}\int d^2\underline{k}_{a0}\frac{\underline{k}_{ab}^2}{\underline{k}_{a0}^2(\underline{k}_{ab}-\underline{k}_{a0})^2}\tilde{F}(x,\underline{k}_{ab}). \qquad (B-31)$$

Since we calculate the contributions to $\Delta\tilde{F}(x,\underline{k}_{a0})$, we should make the replacement $b \leftrightarrow 0$ in Eq. (B-30). Combining the real and virtual parts of the evolution equation, we have

$$-x\frac{\partial\tilde{F}(x,\underline{k}_{a0})}{\partial x}$$
$$= \frac{\alpha_s N_c}{2\pi^2}\int d^2\underline{k}_{ab}\left[2\frac{\underline{k}_{ab}^2}{\underline{k}_{a0}^2\underline{k}_{0b}^2}\tilde{F}(x,\underline{k}_{ab}) - \frac{\underline{k}_{a0}^2}{\underline{k}_{ab}^2\underline{k}_{0b}^2}\tilde{F}(x,\underline{k}_{a0})\right]. \qquad (B-32)$$

According to Eq. (B-18), the distribution $f(x,\underline{k})$ in the TOPT-form contains a singular factor $1/\underline{k}^4$, which arises from the off energy-shell effect in the square of the energy denominator. In order to ensure the safety of taking the $W-W$ approximation, we remove this factor to the evolution kernel and use the following new definition of the unintegrated gluon distribution

$$F(x,\underline{k}) = \frac{\underline{k}^4}{\hat{\underline{k}}^4}\tilde{F}(x,\underline{k}), \qquad (B-33)$$

where $\hat{\underline{k}}$ is a unity vector on the transverse momentum space. Thus, Eq. (B-32) becomes

$$-x\frac{\partial F(x,\underline{k}_{a0})}{\partial x}$$
$$= \frac{\alpha_s N_c}{2\pi^2}\int d^2\underline{k}_{ab}\frac{\underline{k}_{a0}^2}{\underline{k}_{ab}^2\underline{k}_{0b}^2}\left[2F(x,\underline{k}_{ab}) - F(x,\underline{k}_{a0})\right], \qquad (B-34)$$

which consists with a usual form of the BFKL equation.

The correlations among the initial gluons can be neglected in the dilute parton system. In this case the contributions of the interference diagrams Figs. 15c and 15d disappear. Thus, the kernel (B-29) reduces to the splitting functions in the DGLAP equation at the small x limit,

$$\mathcal{K}_{BFKL}(\underline{k}_{ab},\underline{k}_{a0},\alpha_s)\frac{x_1}{x_2}\frac{dx_1}{x_1}d^2\underline{k}_{ab} \to \frac{\alpha_s N_c}{\pi}\frac{dx_1}{x_2}\frac{d\underline{k}^2}{\underline{k}^2}$$

$$\equiv \mathcal{K}_{DGLAP} \frac{d\underline{k}^2}{\underline{k}^2} \frac{dx_1}{x_1}. \qquad (B-35)$$

The two initial gluons have the same transverse momentum and we always can take it to zero and use the collinear factorization to separate the gluon distribution. The corresponding DGLAP equation reads

$$\begin{aligned} Q^2 \frac{\partial g(x_B, Q^2)}{\partial Q^2} &= \int_x^1 \frac{dx_1}{x_1} \mathcal{K}_{DGLAP}\left(\frac{x_B}{x_1}, \alpha_s\right) g(x_1, Q^2) \\ &= \frac{\alpha_s N_c}{\pi} \int_{x_B}^1 \frac{dx_1}{x_1} \frac{x_1}{x_B} g(x_1, Q^2), \end{aligned} \qquad (B-36)$$

where the scaling restriction $\delta(x_2 - x_B)$ is included and Eq. (3) is used.

The above derivations reveal a relation between two evolution equations from a new view point: the BFKL equation dominates the evolutions at the small x regime, where the initial partons appear in the dipole picture. On the other hand, the parton densities become dilute at the larger x regime. In this case, the dipole decomposes to the isolate partons and the BFKL kernel reduces to the DGLAP kernel due to the interferant part of the BFKL kernel disappears.

Appendix C:

We compare the solutions of the following DGLAP equation

$$-x\frac{\partial F(x,k_t^2)}{\partial x} = \frac{\alpha_s N_c}{\pi}\int_{k_{1t,min}^2}^{k_t^2}\frac{dk_{1t}^2}{k_{1t}^2}F(x,k_{1t}^2), \qquad (C-1)$$

with that of the BFKL equation (28) using the same input (33), to illustrate that the linear terms of Eq. (21) is a reasonable form of the DGLAP equation at the DLL approximation. The solid and dashed curves in Figs. 18 and 19 show the unintegrated gluon distributions in the DGLAP (C-1) and BFKL (28) equations, respectively. One can find that the emissive gluons are random walk in k_t-space in the BFKL evolution, while they are ordered in k_t in the DGLAP evolution. In consequence, the distribution steeply increase at small x in the BFKL equation more than that in the DGLAP equation.

References

[1] K. Adcox et al. (PHENIX), Phys. Rev. Lett. 88 (2002) 022301.

[2] K. Aamodt, et. al., [ALICE Collaboration], arXiv:1012.1004.

[3] M. Arneodo, Phys. Rep. 240 (1994) 301.

[4] N.N. Nikolaev and V.I. Zakharov, Phys. Lett. B55 (1975) 297 .

[5] J. W. Cronin, H. J. Frisch, M. J. Shochet, J. P. Boymond, R. Mermod, P. A. Piroue and R. L. Sumner, Phys. Rev. D11 (1975) 3105.

[6] B. B. Back et al. [PHOBOS Collaboration], Phys. Rev. Lett. 91 (2003) 072302; S. S. Adler et al. [PHENIX Collaboration], Phys. Rev. Lett. 91 (2003) 072303; J. Adams et al. [STAR Collaboration], Phys. Rev. Lett. 91 (2003) 072304; I. Arsene et al. [BRAHMS Collaboration], Phys. Rev. Lett. 91 (2003) 072305.

[7] J.Jalilian-Marian, A. Kovner, L. McLerran and H. Weigert, Phys. Rev. D55 (1997) 5414; J.Jalilian-Marian, A. Kovner, A. Leonidov and H. Weigert, Nucl. Phys. B504 (1997) 415; ibid., Phys. Rev. D59 (1999) 014914; E. Iancu, A. Leonidiv and L. McLerran, Nucl. Phys. A692 (2001), 583; ibid., Phys. Lett. B510 (2001) 133.

[8] W. Zhu, D.L. Xu, K.M. Chai and Z.X. Xu, Phys. Lett. B317 (1993) 200; W. Zhu, K.M. Chai and B. He, Nucl. Phys. B427 (1994) 525; W. Zhu, K.M. Chai and B. He, Nucl. Phys. B449 (1995) 183.

[9] F. Gelis and J. Jalilian-Marian, Phys. Rev. D67 (2003), 074019; E. Iancu, K. Itakura, D. N. Triantafyllopoulos, Nucl.Phys. A742 (2004) 182; D. Kharzeev, Y. V. Kovchegov, K. Tuchin, Phys.Lett. B599 (2004) 23; E. Cattaruzza, D. Treleani, Acta Phys. Polon. B36 (2005) 575.

[10] A. H. Mueller, Nucl. Phys. B335 (1990) 115.

[11] L. D. McLerran and R. Venugopalan, Phys. Rev. D49 (1994) 2233; ibid., Phys. Rev. D49 (1994) 3352.

[12] J. L. Albacete, N. Armesto, A. Kovner, C. A. Salgado, U. A. Wiedemann, Phys. Rev. Lett. 92 (2004) 082001.

[13] K. J. Eskola, H. Paukkunen, C. A. Salgado, JHEP 0807 (2008) 102; ibid., JHEP 0904 (2009) 065.

[14] G. Altarelli and G. Parisi, Nucl. Phys. B126 (1977) 298; V.N. Gribov and L.N. Lipatov, Sov. J. Nucl. Phys. 15 (1972) 438; Yu.L. Dokshitzer, Sov. Phys. JETP. 46 (1977) 641.

[15] E.R. Cazaroto, F. Carvalho, V.P. Goncalves, F.S. Navarra, Phys. Lett. B669 (2008) 331; C. Brenner Mariotto, V. P. Goncalves, Phys. Rev. C78 (2008) 037901.

[16] L.V. Gribov, E.M. Levin and M.G. Ryskin, Phys. Rep. 100 (1983) 1.

[17] A.H. Mueller and J. Qiu, Nucl. Phys. B268 (1986) 427.

[18] K.J. Eskola, J.W. Qiu and X.N. Wang, Phys. Rev. Lett. 72 (1994) 36; K.J. Eskola, H. Honkanen, V.J. Kolhinen, J.W. Qiu and C.A. Salgado, Nucl. Phys. B660 (2003) 211.

[19] W. Zhu, Nucl. Phys. B551 (1999) 245.

[20] W. Zhu and J.H. Ruan, Nucl. Phys. B559 (1999) 378; W. Zhu and Z.Q. Shen, HEP & NP, 29 (2005) 109.

[21] K. Kogut and L. Susskind, Phys. Rev. D9 (1974) 697.

[22] J.H. Ruan and W. Zhu, Phys. Rev. C80 (2009) 045209.

[23] L.N. Lipatov, Sov. J. Nucl. Phys. 23 (1976) 338; V. S. Fadin, E.A. Kuraev and L.N. Lipatov, Phys. Lett. B60 (1975) 50; E.A. Kuraev, L.N. Lipatov and V. S. Fadin, Sov. Phys. JETP 44 (1976) 443; E.A. Kuraev, L.N. Lipatov and V. S. Fadin, Sov. Phys. JETP 45 (1977) 199; I. I. Balitsky and L.N. Lipatov, Sov. J. Nucl. Phys. 28 (1978) 822; I. I. Balitsky and L.N. Lipatov, JETP Lett. 30 (1979) 355.

[24] M. Ciafaloni, Nucl. Phys. 296 (1988) 49; S. Catani, F. Fiorani and G. Marchesini, Phys. Lett. B234 (1990) 339; Nucl. Phys. 336 (1990) 18.

[25] A.J. Askew, J. Kwiecinski, A.D. Martin and P.J. Sutton, Phys. Rev. D47 (1993) 3775.

[26] W. Zhu, J.H. Ruan, J.F. Yang and Z.Q. Shen, Phys. Rev. D68 (2003) 094015.

[27] M.Derrick et al, Zeit.Phys. C72 (1996) 399; A.C.Benvenuti et al, Phys.Lett. B223 (1989) 485.

[28] CERN NA28/EMC, M. Arneodo et. al., Phys. Lett. B211 (1988) 493; Nucl. Phys. B333 (1990) 1.

[29] CERN NA37/NMC, P. Amaudruz et. al., Nucl. Phys. B441 (1995) 3.

[30] A. Bodek (SLAC E139), talk at the Lepton-Photon Symposium and Europhysics Conference on High Energy Physics LP-HEP91, Geneva, Switzerland, 25th July-1st August 1991.

[31] CERN NA37/NMC, P. Amaudruz et. al., Nucl. Phys. B371 (1992) 553.

[32] M. Hirai, S. Kumano, T. H. Nagai and K. Sudoh, Phys. Rev. D75 (2007) 094009.

[33] X. N. Wang, Z. Huang and I. Sarcevic, Phys. Rev. Lett. 77 (1996) 231; X. N. Wang and Z. Huang, Phys. Rev. C55 (1997) 3047; X. N. Wang, Nucl.Phys. A702 (2002) 238.

[34] C.F. von Weizsäcker, Z. Phys. 88 (1934) 612; E.J. Williams, E.J., Phys. Rev. 45 (1934) 729; P. Kessler, Nuovo Comento 16 (1966) 809; V.N Baier, V.S. Fadin and V.A. Khoze, Nucl. Phys. 65 (1973) 381; M.S. Chen and P. Zerwas, Phys. Rev. D12 (1975) 187.

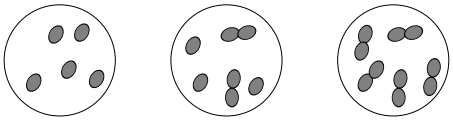

Fig. 1 The illustrating kinematic regions of the DGLAP- and BFKL equations.

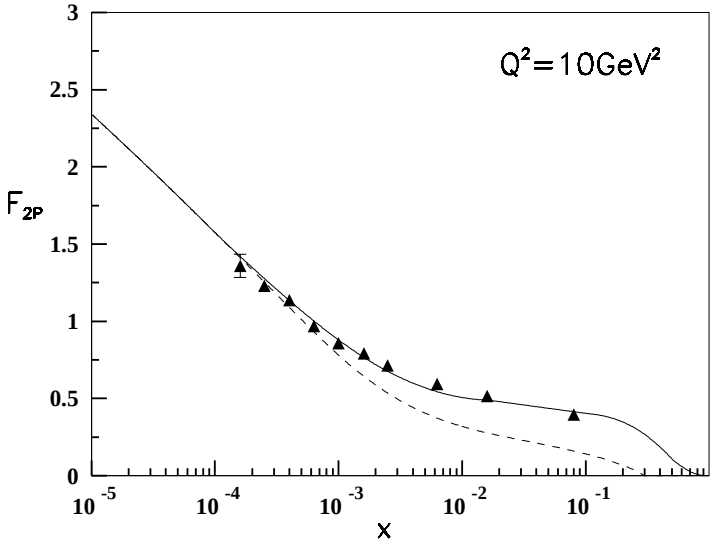

Fig. 2 The fit of the computed $F_{2P}(x, Q^2 = 10\ GeV^2)$ in proton by the evolution equations (21), (29) and (32) using the input Eq. (33) (dashed curve). The contributions of the valence quarks are parameterized by the differences between solid and dashed curves. The data are taken from Ref. [27].

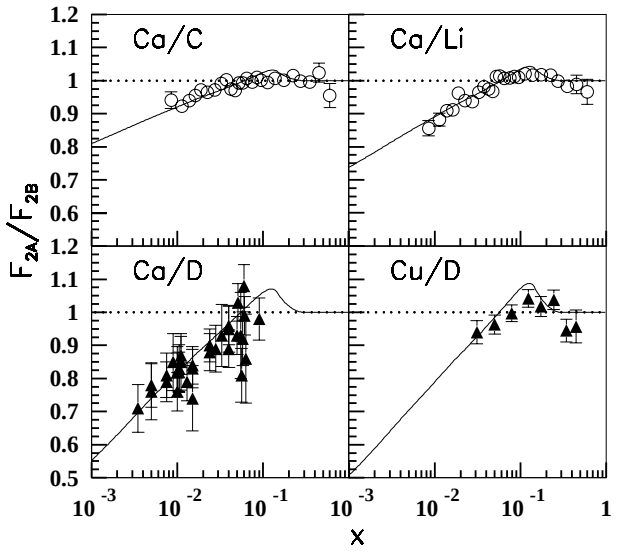

Fig. 3 Predictions of the evolution equations (21), (22) and (29) compared with the EMC ratio of the structure functions for various nuclei. The data are taken from [28,29]. All curves are for $Q^2 = 10\ GeV^2$

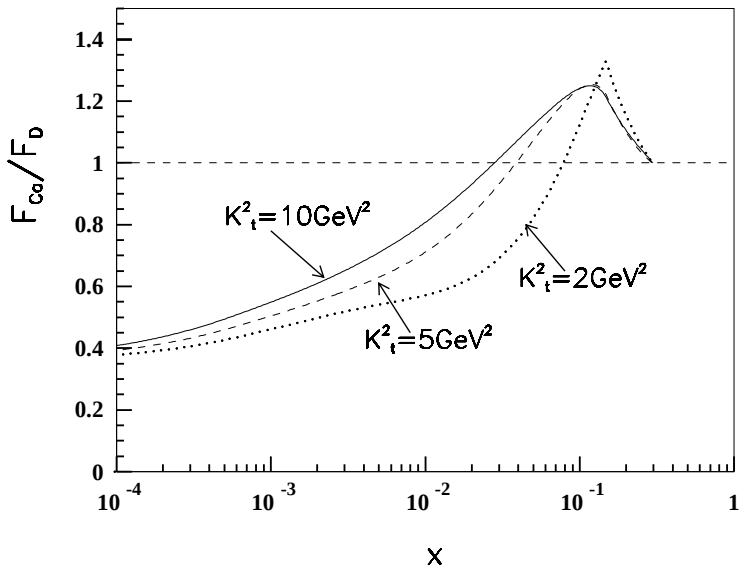

Fig. 4 Predictions of the evolution equations (21), (22) and (29) for the ratio of the unintegrated gluon distributions in Ca/D with different values of x and given k_t.

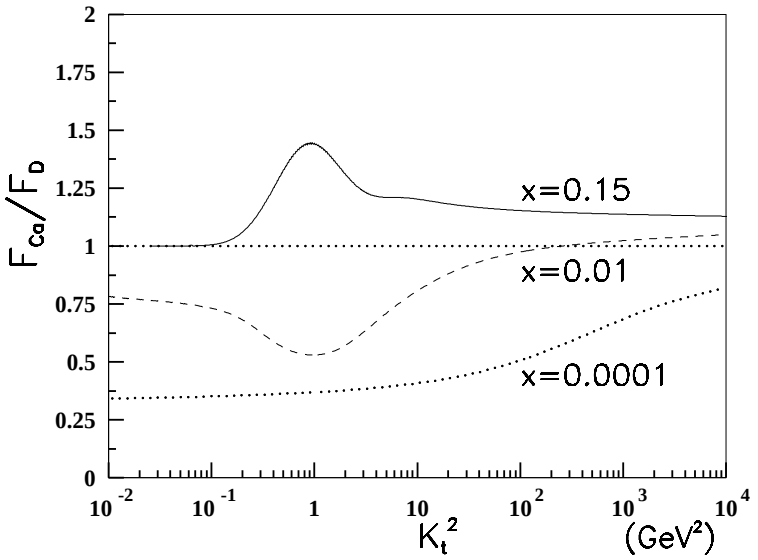

Fig. 5 Similar to Fig. 4 but with different values of k_t and given x.

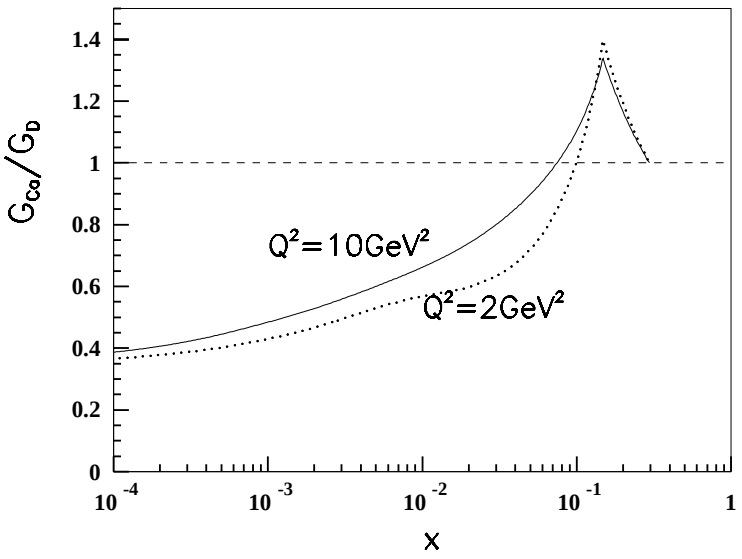

Fig. 6 x-dependence of the ratio for the integrated gluon distributions in Ca/D in the evolution equations (21), (22) and (29).

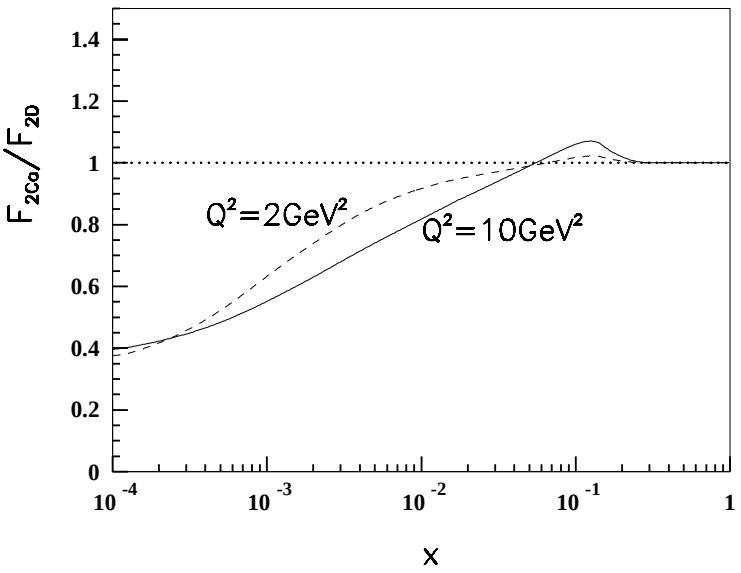

Fig. 7 Similar to Fig. 6 but for the the ratio of the structure functions.

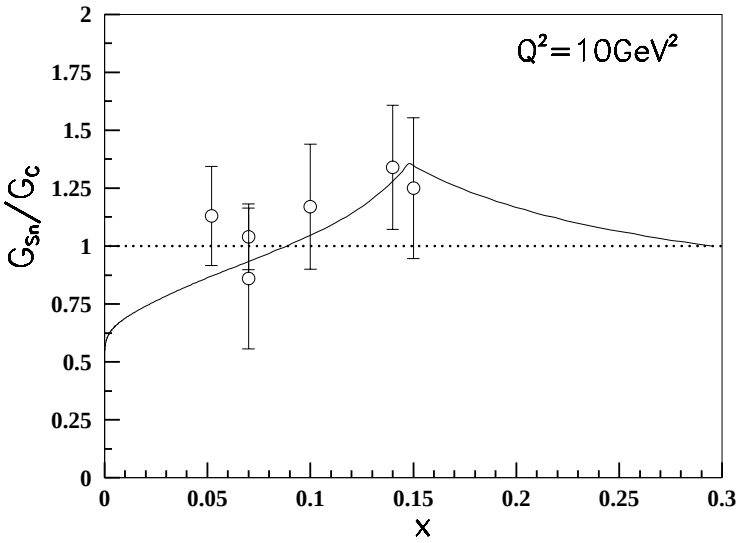

Fig. 8 Predictions for the ratio of the gluon distributions in Sn/C and the data are taken from Ref. [31].

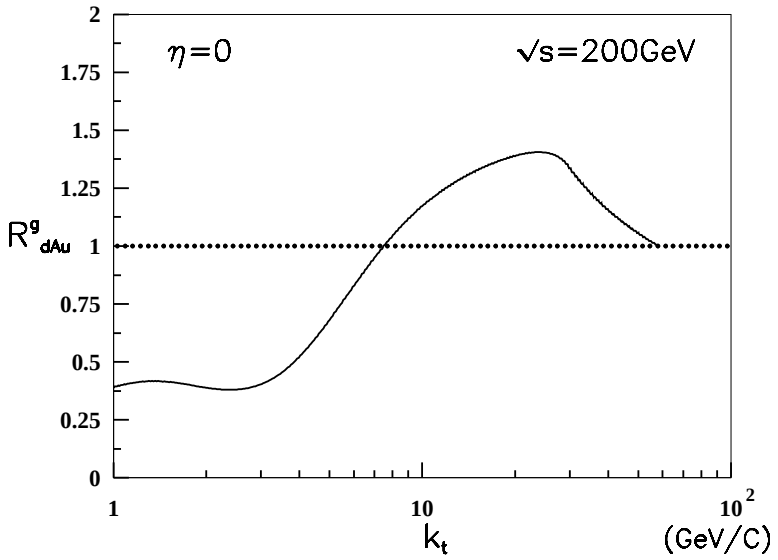

Fig. 9 Predicted nuclear modification factor R^g_{dAu} of gluon jet in central $d + Au$ collisions at $\sqrt{s} = 200GeV$.

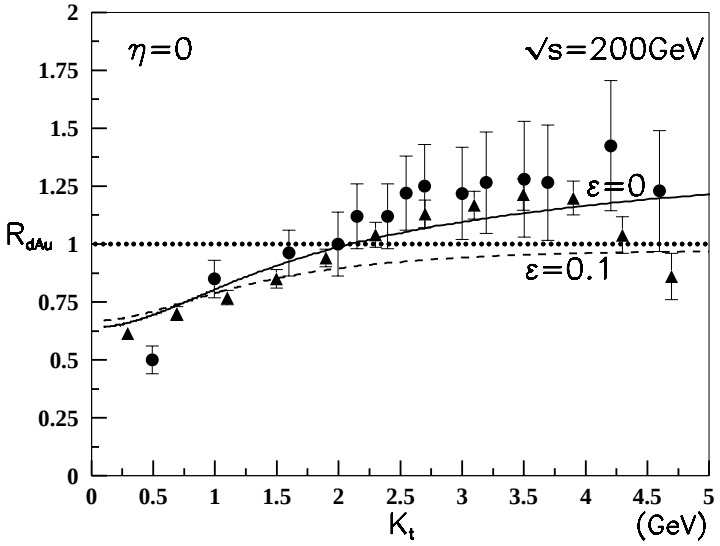

Fig. 10 Nuclear modification factor R_{dAu} of charged particles in central d+Au collisions at $\sqrt{s} = 200GeV$, where fractional energy loss $\epsilon = 0$ (solid curve) and 0.1 (dashed curve). The data are taken from Ref. [1].

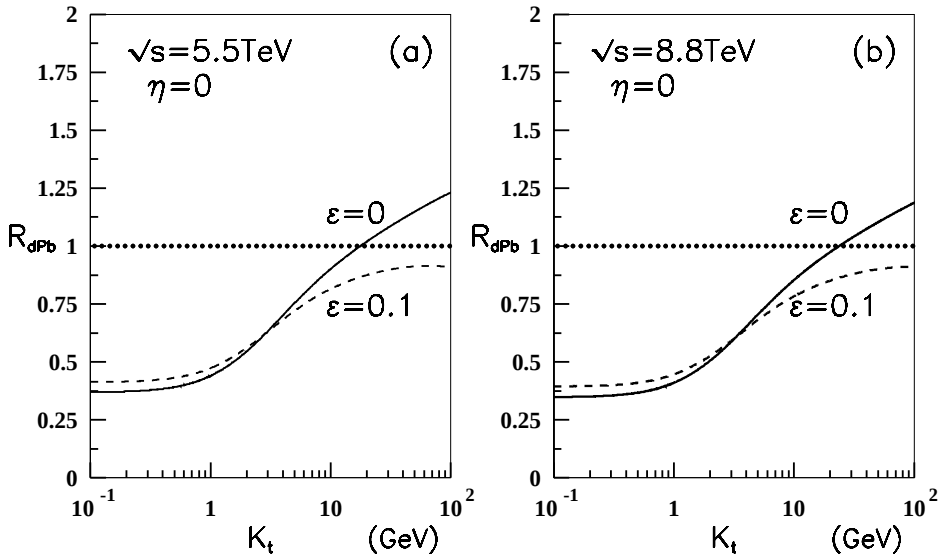

Fig. 11 Predicted nuclear modification factor R_{dPb} of charged particles in central $d+Pb$ collisions at (a) $\sqrt{s}=5.5TeV$ and (b) $8.8TeV$.

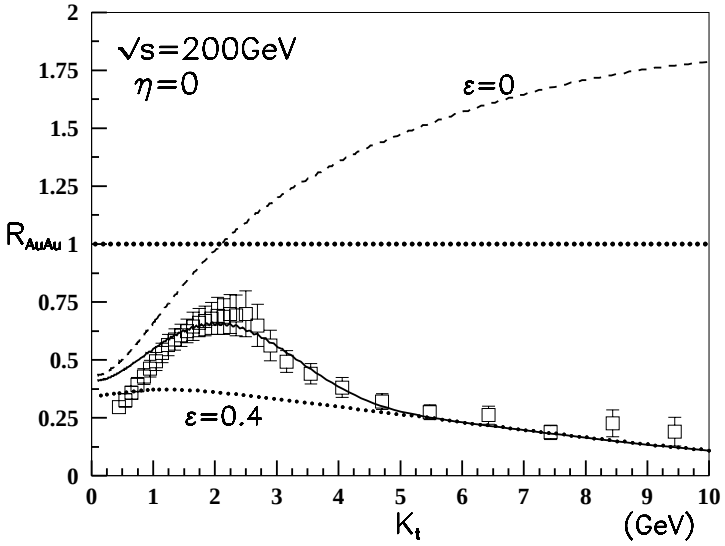

Fig. 12 Estimated nuclear suppression factor R_{AA} in central $Au + Au$ collisions at $\sqrt{s} = 200GeV$: solid curve using Eq. 46 with $a = 0.2$, $b = 0.4$, (see Fig. 13a); dashed curve using $\epsilon = 0$, and pointed curve using $\epsilon = 0.4$. The data are taken from Ref. [1].

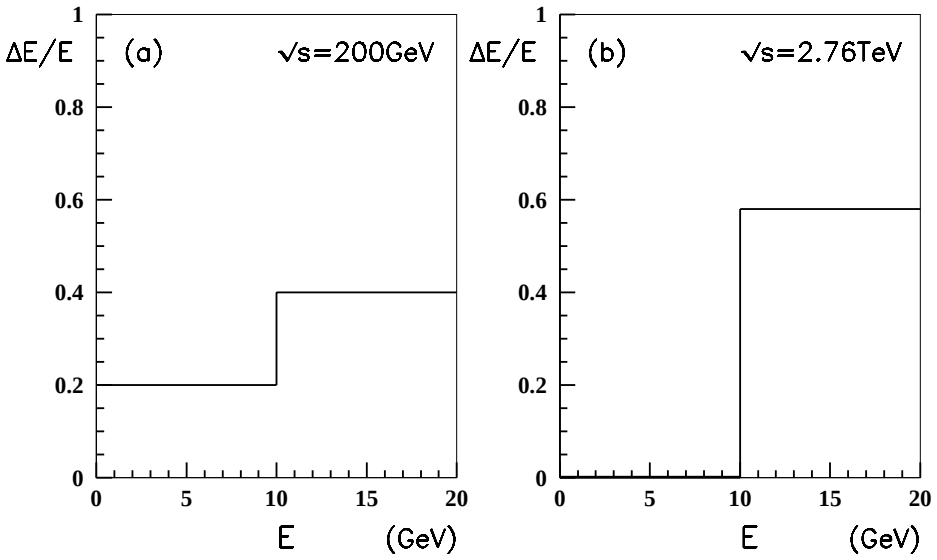

Fig. 13 Two possible fractional energy losses, which correspond to (a) central collisions at $\sqrt{s} = 200GeV$ for $Au + Au$ and (b) at $\sqrt{s} = 2.76TeV$ for $Pb + Pb$, respectively.

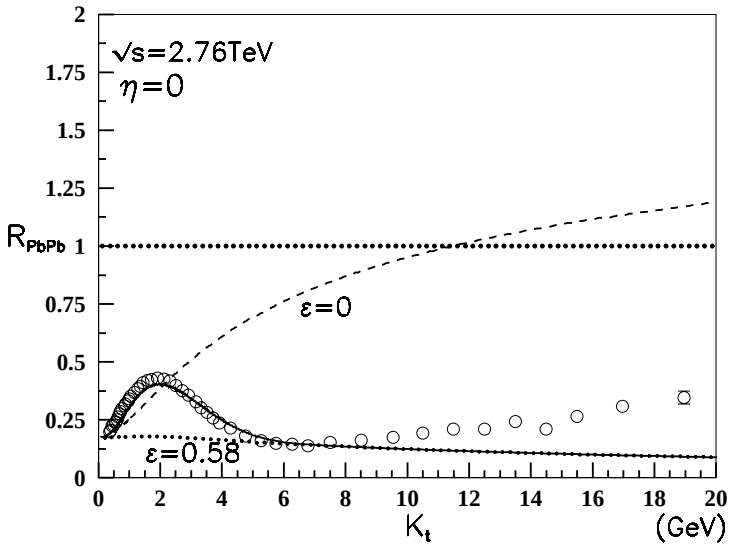

Fig. 14 Similar to Fig. 12, but for central $Pb+Pb$ collisions at $\sqrt{s} = 2.76TeV$, where solid curve using Eq. 46 with $a = 0$, $b = 0.58$, (see Fig. 13b); dashed curve using $\epsilon = 0$, and pointed curve using $\epsilon = 0.58$. The data are taken from Ref. [2].

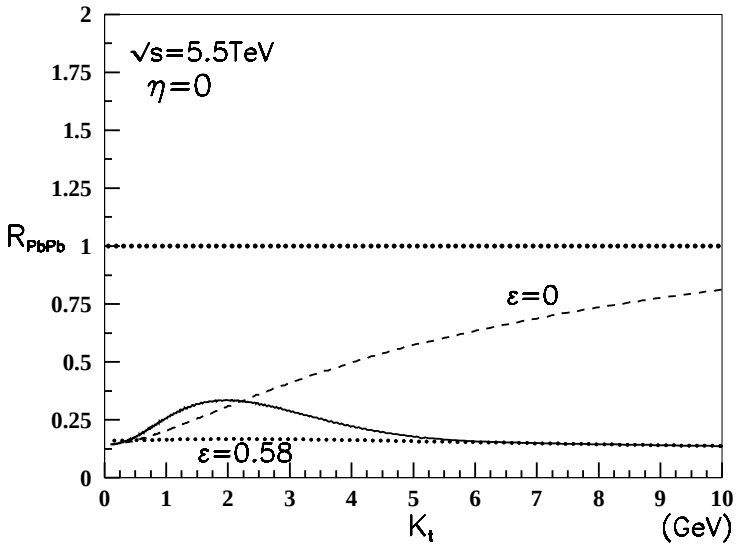

Fig. 15 Predicted nuclear suppression factor R_{AA} in central $Pb + Pb$ collisions at $\sqrt{s} = 5.5TeV$, all parameters are same as Fig. 14.

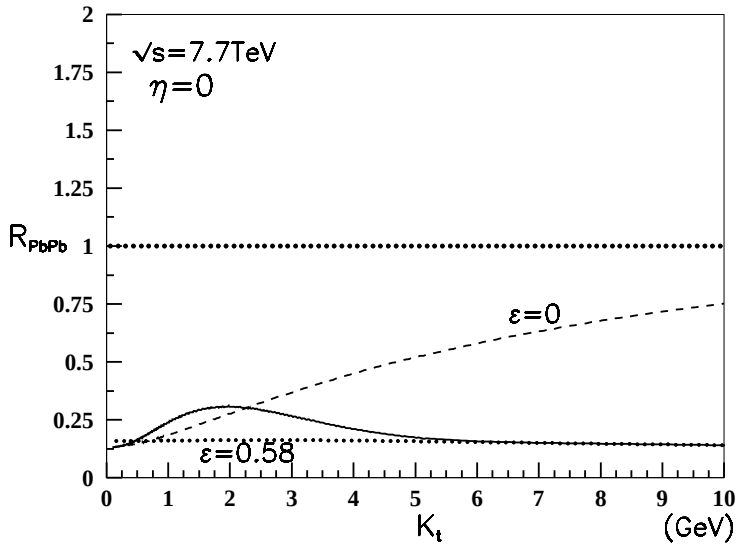

Fig. 16 Predicted nuclear suppression factor R_{AA} in central $Pb + Pb$ collisions at $\sqrt{s} = 7.7TeV$, all parameters are same as Fig. 14.

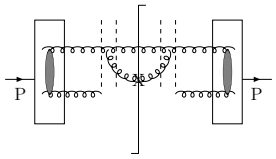

(a)

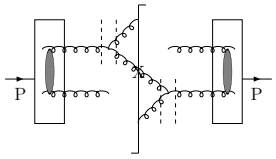

(b)

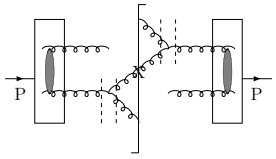

(c)

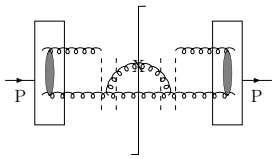

(d)

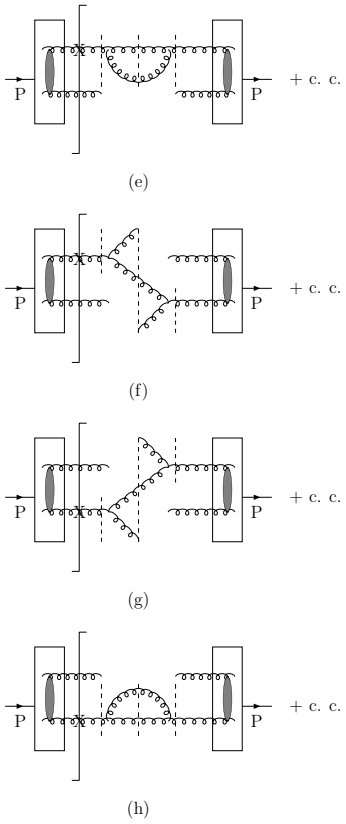

Fig. 17 The TOPT-diagrams, which lead to BFKL equation. The dashed lines are the time ordered lines in the TOPT.

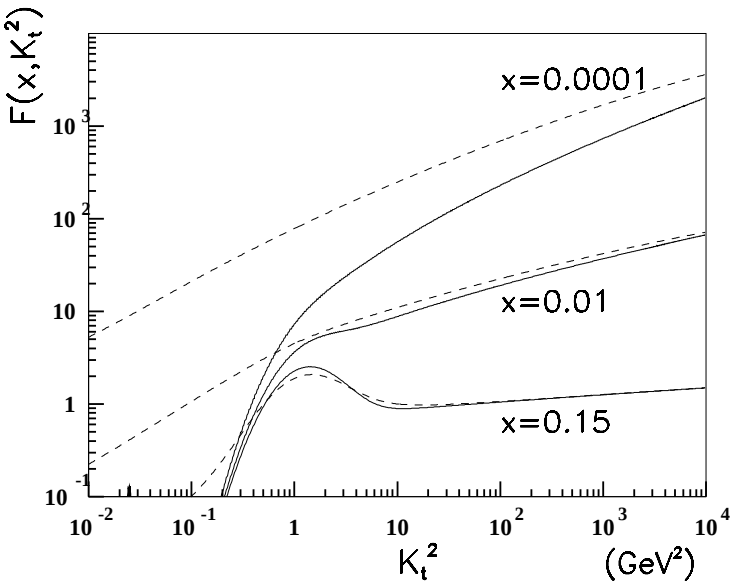

Fig. 18 The k_t^2-dependence of the unintegrated gluon distribution with different values of x in the linear part of Eq. (21) (solid curves) and BFKL equation (dashed curves).

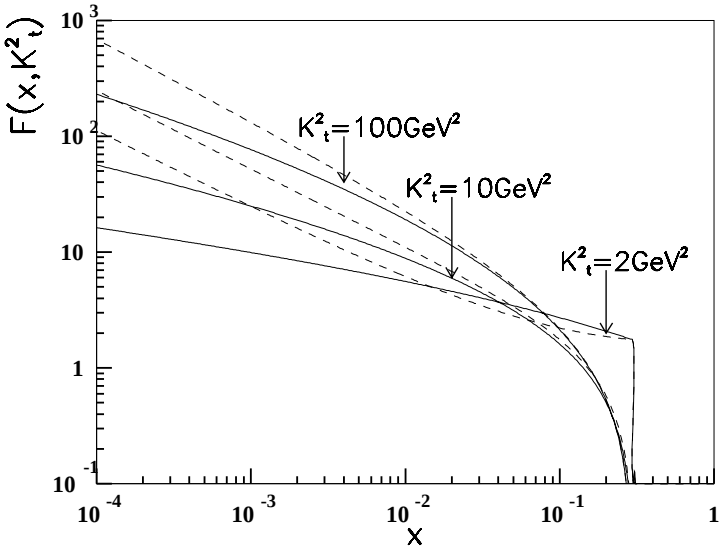

Fig. 19 Similar to Fig. 18 but for the x-dependence with different values of k_t .